

1 **Engineered/designer hierarchical porous carbon materials for organic**
2 **pollutant removal from water and wastewater: A critical review**

3
4 Mengxue Zhang^{a,b,1}, Avanthi Deshani Igalavithana^{a,1}, Liheng Xu^b, Binoy Sarkar^c, Deyi Hou^d,
5 Ming Zhang^{b,¶}, Amit Bhatnagar^c, Won Chul Cho^f, Yong Sik Ok^{a,*}

6
7 ^aKorea Biochar Research Center & Division of Environmental Science and Ecological
8 Engineering, Korea University, Seoul, Republic of Korea

9 ^bDepartment of Environmental Engineering, China Jiliang University, No. 258, Xueyuan
10 Street, Hangzhou, Zhejiang 310018, P.R. China

11 ^cLancaster Environment Centre, Lancaster University, Lancaster, LA1 4YQ, United Kingdom

12 ^dSchool of Environment, Tsinghua University, Beijing, 100084, P.R. China

13 ^eDepartment of Environmental and Biological Sciences, University of Eastern Finland, P.O.
14 Box 1627, FI-70211 Kuopio, Finland

15 ^fHydrogen Laboratory, Korea Institute of Energy Research (KIER), Daejeon, Republic of
16 Korea

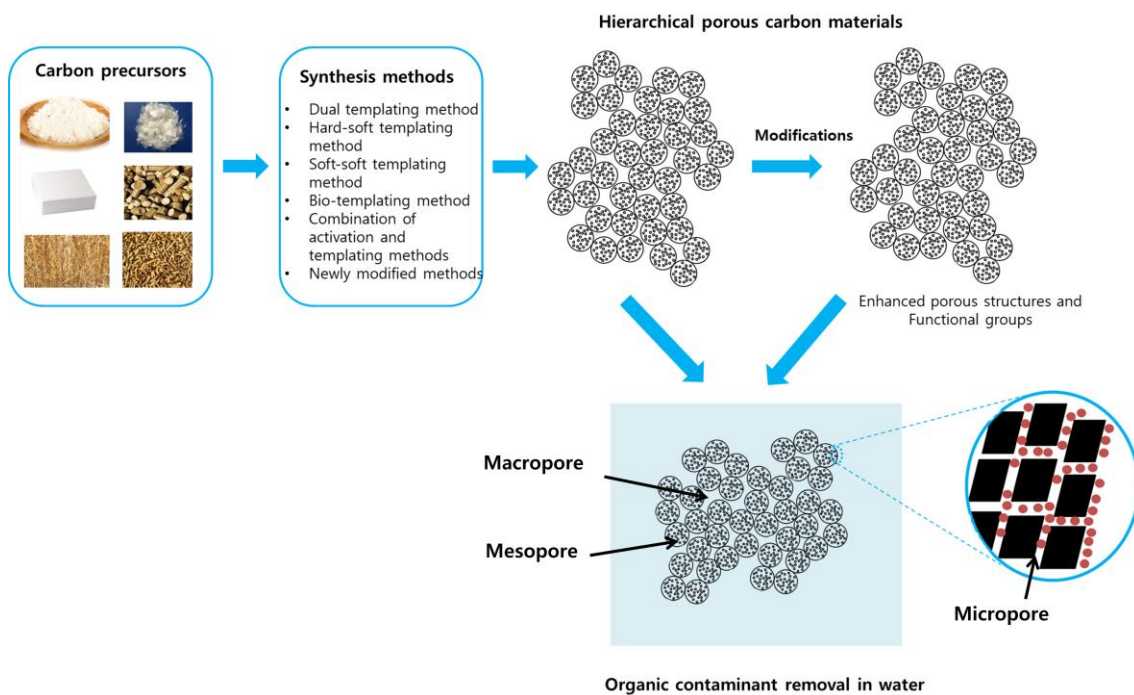
17
18 *Corresponding Author Email: yongsikok@korea.ac.kr

19 [¶]Co-corresponding Author Email: zhangming@cjlu.edu.cn

20 ¹These authors contributed equally to this paper as first authors.

21

22 **Graphical abstract**



23

24

25 **Highlights**

26 Hierarchical porous carbon materials (HPCs) are important in different disciplines.

27 HPCs can be synthesized from diverse carbon materials by various methods.

28 HPCs are highly effective in organic contaminant removal in waters.

29 The efficacy of organic contaminant removal can be enhanced by modification of HPCs.

30 **Abstract**

31 Hierarchical porous carbon (HPC) materials have found advanced applications in energy
32 storage, adsorption, and catalysis in recent years. Since HPCs can be synthesized from a vast
33 range of inexpensive carbon precursors including waste biomasses, and contain unique
34 structural features, such as nano-scale dimension, high porosity, high surface area, and
35 tunable pore surfaces, these materials hold an immense potential for removing contaminants
36 from water. However, currently this area is severely under-explored. In this review, we
37 discussed the recent advances of synthesis, modification, and application of HPCs for
38 contaminated water cleanup, especially focusing on organic pollutants. Findings suggest that
39 HPCs can be synthesized using multiple methods (e.g., dual templating, hard-soft templating,
40 soft-soft templating, bio-templating, a combination of activation and templating) including
41 the advanced nanopore lithography technique. Owing to their intrinsic hydrophobic nature
42 and unique interconnected porous structure, HPCs demonstrate high affinity to hydrophobic
43 organic contaminants, which can be enhanced many folds by target-specific chemical
44 activation such as alkali and/or hydrothermal treatments. Successful high-performance
45 removal of water contaminants by pristine and modified HPCs include plastic-derived (e.g.,
46 bisphenol A), pharmaceutical (e.g., antibiotics), dye (e.g., methylene blue) and pesticide
47 micro-pollutants. Besides, the easily tunable features of HPCs make them a promising
48 commercial filtration/membrane material for household and large-scale wastewater treatment
49 applications. Therefore, future research is warranted to find optimal and effective HPC
50 synthesis and modification methods for further improving their ability to remove aqueous
51 organic contaminants as a low-cost and energy-inexpensive remediation technology.

52

53 **Keywords:** Carbon material; Contamination; Engineered carbon; Electrode material; Waste
54 water treatment.
55

56 **1. Introduction**

57 Hierarchical porous carbon (HPC) materials have drawn increasing attention over the
58 past twenty years [1–3]. HPCs with hierarchical pores can be synthesized from carbon
59 precursors via chemical activation and templating with different materials. Scientists around
60 the world are formulating, testing, and applying HPCs, derived from many different carbon
61 precursors, such as kraft lignin [4], polyacrylonitrile [5], cotton stalk [6], chitosan [7], and
62 polystyrene [8] in different applications.

63 HPCs have many tailored structural features, such as nanostructures, high porosity, high
64 surface area, unique pore surface chemistry, and high electrical conductivity [9–11].
65 Consequently, HPCs can be used in different real-world applications, such as, electrode
66 materials, electro-catalysts, energy storage, chromatography, adsorption, catalyst, sensing and
67 nanoreactors [2,12–16].

68 Water pollution by organic contaminants has been repeatedly reported globally [17]. For
69 instance, discharge of pharmaceuticals and personal care products from untreated or poorly
70 treated wastewaters around the world has been identified as one of the emerging water
71 polluting problems [18–24]. Subsequently, the scarcity of clean water and high demand of
72 water consumption in the world need effective remediation technologies and pollution control
73 measures [25–28]. With interconnected porous structures, tunable pore size and structures,
74 excellent flow-through permeability, high specific surface area (SSA), HPCs are one of the
75 best materials that can effectively be used in water remediation [2,29].

76 There are 3892 articles published in SCOPUS database (quoted on 15 January 2020) on
77 HPCs when searched in article title, abstract and keywords. Among them, 1.7% are review
78 articles, and >70% of the review articles are focused on advanced applications of HPCs, such

79 as super capacitor, energy storage and catalysis [30–32]. However, according to the SCOPUS
80 database and to the best of authors' knowledge, no review till date concentrated on the
81 removal of aqueous organic contaminants by HPCs. Applications of HPCs in water related
82 studies have increased only since 2010 (Fig. 1). Hence, understanding the synthesis
83 procedures of HPCs, their properties, and possible modifications are critical to promote their
84 applications in water and wastewater treatment. Therefore, this work will provide the first
85 critical review on the designs and applications of HPCs for the removal of organic
86 contaminants from polluted waters.

87

88 **2. Methods of synthesizing HPCs**

89 **2.1. Dual templating method**

90 Templating is the most commonly and effectively used method to design and control pore
91 size distributions of HPCs (Table 1). Knox et al. [33] pioneered the method to synthesize
92 porous carbon materials by the templating method, and since then, it has been gradually
93 developed. Templating method refers to the process of first depositing related materials into
94 the holes or surface of the template by physical or chemical ways, and then removing the
95 template to obtain nanomaterials with standard morphology and size of the template. The
96 process proceeds in the area of effective control, and thus, it is easy to tail and vary the
97 structural parameters of HPCs. Templating methods mainly include hard and soft template
98 methods (Fig. 2).

99 Hard templates are generally rigid forms, held together by stable inorganic solids [1]. The
100 inorganic solids can be different types of silica, such as silica monolith [34], silica spheres
101 [35], silica colloidal crystals [36,37], silica opal [38,39], etc. In addition, CaCO₃ [40] and

102 Na_2CO_3 [41] are also commonly used as porogen of hard template. Soft templates are
103 typically organic polymers that can be thermally decomposed and removed [1,42,43]. These
104 thermally decomposed polymers can be polystyrene (PS) [44,45], polymethyl methacrylate
105 (PMMA) [46], polyurethane (PU) and surfactants [47].

106 Considering that HPCs are composed of different levels of pores, the dual templating
107 method is commonly used to synthesize HPCs of macro-mesoporous, meso-microporous,
108 macro-meso-microporous structures. The carbon source is guided by the double space
109 limiting action of two pore-forming agents to achieve the purpose of the graded structure.

110

111 **2.2. Hard-soft templating method**

112 When combining hard and soft templates, phenolic resin is often used as the carbon
113 precursor to allow the organic-organic self-assembly with triblock copolymers in the
114 interspaces between inorganic solids [36]. Silica is still one of the most popular hard template
115 to synthesize mesoporous or macroporous carbons with diameters of about 30-50 nm [48] or
116 200-500 nm [35,36] because it is easy to control the ordered structure. In addition, hard silica
117 template can restrict the shrinkage of the framework during the thermosetting and
118 carbonization process [36,49]. For example, Yonghui et al. [36] assembled purified and
119 uniform silica microspheres into ordered colloidal crystal templates, then heated at 100 °C for
120 24 h to ensure the structural hierarchy and stability of templates. The obtained porous carbons
121 had a highly ordered face-centered cubic macrostructure with tunable pore sizes of 230-430
122 nm and interconnected windows with a size of 30-65 nm [36]. Besides, Li et al. [38] explored
123 the effect of silica to the restrain shrinkage of mesoporous polymers. The authors indicated

124 that the hydroxyl group interactions among the resin polymer and the surface of SiO₂ spheres
125 and 3D structure of SiO₂ template played important roles in restrain shrinkage [38].

126 Furthermore, by using two diameter-sized colloidal crystal templates, 3D interconnected
127 ordered macroporous carbon with uniform mesoporous walls are fabricated. The process is
128 realized through physical mixing of polystyrene (PS) colloidal crystals and silica particles,
129 which simplifies the template synthesis route. Chai et al. [44] prepared HPCs using nano-
130 casting method. First, PS microspheres and small silica particles were mixed. During the
131 drying process of the mixture, PS microspheres self-assembled into an ordered array, while
132 SiO₂ particles with small size were closely arranged in the cracks of PS array, forming a
133 mixed dual-template. The carbonization and removal of PS template created templated
134 aggregate of the small silica particles, which was then impregnated with the carbon precursor
135 (divinylbenzene), and finally HPCs were obtained through the carbonization of the carbon
136 precursor and dissolution of silica (Chai et al., 2004).

137 In a different study, Woo et al. [45] used PS colloidal crystals as a pore-making agent as
138 well as a carbon precursor. After heat treatment at 300 °C, the melted PS was first penetrated
139 into the space between the colloidal silica. The penetrated PS was then carbonized with heat
140 treatment to provide a very thin carbon layer on the colloidal silica, and the microporous
141 structure corresponding to the PS particle size was formed simultaneously. This greatly
142 simplified the process of the impregnation of carbon precursor [45].

143 Zhang et al. [50] developed a one-pot method to avoid pre-synthesis of the template and
144 additional infiltration. The interconnected macropores and mesopores were synthesized by in-
145 situ self-assembly of colloidal polymer and SiO₂ particles with sucrose as the carbon source.
146 This procedure is simple and easy to operate. In addition, intermediate composite films are

147 compounded rather than powder due to soft polymer spheres ($T_g = 21\text{ }^\circ\text{C}$) compared with
148 hard PS spheres. It is the surrounding nano-silica particles and sucrose crystallites that
149 restrain the deformation of these soft polymer spheres [50].

150

151 **2.3. Soft-soft templating method**

152 Unlike the hard templates, the soft templates can be removed in the process of
153 carbonization, and the use of harmful reagents for etching the templates can be reduced to
154 some extent. For instance, two soft templates of poly(methyl methacrylate) (PMMA)
155 colloidal crystals and triblock copolymer can be used to prepare HPCs [51]. In this process,
156 PMMA plays the same role as silica, while the PMMA template can be decomposed
157 completely during carbonization when the temperature reaches $900\text{ }^\circ\text{C}$ to produce macropores
158 [51]. Lower concentration of amphiphilic triblock copolymer can produce surface-centered
159 cubic mesoporous structures, and a higher concentration can produce 2-D mesoporous
160 structures [51].

161 Similarly, Xue et al. [52] used organic polyurethane (PU) foam scaffold as a sacrificial
162 macroporous template on which solvent evaporation induced the self-assembly process of
163 phenol/formaldehyde resol and triblock copolymer. Their hierarchical porous framework
164 constructed by macropores was cable-like struts, and the carbon material exhibited relatively
165 disordered macropores with diameters of about $100\text{-}450\text{ }\mu\text{m}$ [52].

166

167 **2.4. Bio-templating method**

168 Unlike previously discussed methods that use artificial carbon skeletons, bio-templating is
169 a simple, sustainable, environment-friendly and suitable method for mass production of HPCs.

170 Biomass of natural inorganic/organic composites often contains nanostructures. For example,
171 Huang and Doong [53] prepared HPCs by employing natural sugarcane bagasse. Surface
172 coating (i.e., triblock copolymer F127 and phenol–formaldehyde resin) and solvent
173 evaporation-induced self-assembly were employed. After carbonization at 1000 °C, the
174 carbon materials formed from sugarcane bagasse maintained a stable skeleton structure, and
175 interconnected macropores based on the natural texture and 2-D hexagonal ordered
176 mesopores were clearly observed. The authors suggested that this might be due to the
177 hydroxyl functional groups of the bagasse which interacted with phenolic resin. The
178 drawback was that the specific surface area (SSA) was not high enough, only 544 m² g⁻¹, and
179 the microporosity was up to 66-67% [53].

180 Chen et al. [54] selected fish scales as a raw material to prepare HPCs, which was activated
181 by KOH to produce micropores with SSA as high as 2273 m² g⁻¹. First, the fish scales have an
182 overlapping plywood structure of stratified lamellae, which can be preserved to maintain
183 carbon skeleton after carbonization and activation. Second, the fish scales are composed of
184 organic components (mainly collagen fibers) and inorganic components (calcium-deficient
185 hydroxyapatite), which form macropores and mesopores, respectively. Hydroxyapatite
186 disperses well in organic components helping to maintain the stability of the carbon skeleton
187 [54].

188

189 **2.5. Combination of activation and templating methods**

190 In general, the relatively ordered HPCs, containing a large number of micropores, is
191 mainly prepared by the template method following post-activation step to produce micropore

192 on the walls of mesopore or macropore [1]. Carbon dioxide, water vapor and KOH are
193 commonly used as the physiochemical activation agents [55,56].

194 Xia et al. [57] explored the effects of CO₂ activation on the pore structure of highly ordered
195 mesoporous carbon CMK-1 and CMK-3. The activated carbons showed variable porous
196 textures and remarkable enhancements in the volume and SSA of both mesopores and
197 micropores. The authors indicated that this was probably due to the combined effects of the
198 closed pores, new narrow pores and extensive pre-existent pores. The great enhancement was
199 accompanied by the expansion of the ordered porous structures. With the extension of
200 activation time, the long-range ordering was lost; however, the interconnection of pores in
201 some parts still remained intact [57].

202 Compared with silica, commercial nano-CaCO₃ microspheres have been used as a
203 relatively environmentally-friendly nano-template to synthesize HPCs, and attracted wide
204 attention. Macro-mesoporous and micro-mesoporous carbon can be synthesized by choosing
205 different microsphere sizes of nano-CaCO₃. Yang et al. [58] reported that nano-CaCO₃ could
206 be used not only as a template, but also as an activating agent by producing CO₂ from the
207 carbon precursor to produce micro- and mesopores [58]. Similarly, nano-CaCO₃ was used as
208 a dual template to synthesize macro-mesoporous carbon nanofiber, and CaCO₃ could be
209 dissolved by acid to form macropores after the carbonization [38].

210

211 **2.6. New methods of synthesizing HPCs**

212 In order to overcome the drawbacks of the above-mentioned methods, many novel
213 strategies and raw materials have been introduced to synthesize HPCs. Martín-Jimeno et al.
214 [59] successfully synthesized a 3-4 nm uniform mesoporous carbon material by using metal

215 organic framework (MOF) as a template. They coated the MOF with graphene oxide
216 nanosheets. At high temperatures (i.e., >800 °C), the incipient porosities of MOF served as
217 the entry point for activation and created uniform mesoporosity on the graphene oxide
218 nanosheets. This process can be termed as “nanopore lithography”. The hierarchically micro-
219 mesoporous structure relies on a strictly controlled amount of KOH (activating agent), and
220 excessive activation with high amounts of KOH can cause a collapse of the carbon skeleton
221 [59].

222 Pomelo peel, an environment-friendly biomass, was used to synthesize hierarchical meso-
223 microporous carbon [11]. The dual-activating agent of $\text{NH}_4\text{H}_2\text{PO}_4$ and KHCO_3 suggestively
224 increased the SSA ($2726 \text{ m}^2 \text{ g}^{-1}$) and percentage of mesopores (52%) of HPCs. At an elevated
225 temperature (e.g., 800 °C), the NH_3 , CO and CO_2 gases generated from the activating agents
226 were released to create pores in the carbon precursor. The difference between the two
227 activating agents was that they promoted the expansion of the micropores and the conversion
228 of micropore to mesopore, respectively [11].

229 Siyasukh et al. [60] reported that HPC monolith could be synthesized using high intensity
230 ultrasonic wave to generate macropores, and $\text{Ca}(\text{NO}_3)_2$ impregnation and CO_2 activation
231 could generate mesopores on the wall of macroporous monolith (Siyasukh et al., 2008). Zou
232 et al. [61] reported that HPC could be compounded through the reactions of linear
233 polystyrene resin, carbon tetrachloride and anhydrous aluminum chloride. It was the -CO-
234 group that connected the polystyrene chains and made up the whole carbon structure. The
235 mesopore and macropore were caused by the gap of different sizes formed by the non-
236 uniform arrangement of polystyrene nanoparticles [61].

237

238 3. HPC properties

239 The unique properties of HPCs include uniform macropores, interconnected meso- and/or
240 micropores, and an overall well-defined pore system, which allow them to have an excellent
241 mass transfer performance associated with the larger pores, and abundant adsorption sites
242 associated with the smaller pores. Furthermore, high SSA and pore volume in general, are
243 also crucial to promote mass transfer and adsorption processes. HPCs containing multiple
244 levels of pores have higher SSA and pore volume than the carbon materials with single-size
245 pores due to the fact that the space of HPCs is fully utilized. Li et al. [49] indicated that
246 macro-mesoporous carbon (Pluronic P123 and silica as pore-making agent) has a higher SSA
247 ($803 \text{ m}^2 \text{ g}^{-1}$) and pore volume ($0.86 \text{ m}^3 \text{ g}^{-1}$) than that of pure mesoporous carbon ($350 \text{ m}^2 \text{ g}^{-1}$
248 and $0.35 \text{ m}^3 \text{ g}^{-1}$, respectively). Meanwhile, Zhang et al. [37] reported that macro-mesoporous
249 carbon also had a higher SSA ($1290 \text{ m}^2 \text{ g}^{-1}$) and pore volume ($1.35 \text{ m}^3 \text{ g}^{-1}$) than that of pure
250 macroporous carbon ($473 \text{ m}^2 \text{ g}^{-1}$ and $0.82 \text{ m}^3 \text{ g}^{-1}$, respectively) in the absence of Poloxamer
251 407, used as a mesoporous template.

252 Through self-thermal polymerization of phenolic resin, a highly crosslinked and stable
253 polymer can be formed, leading to the monolithic feature of cm in size (Li et al., 2016; Meng
254 et al., 2005). In the absence of surfactant to build a stable structure, the synthesized thin films
255 or powders might have macroscopic morphology. However, in practical water treatment
256 process, these hierarchically porous carbon monoliths (HPCM) would show great advantages
257 over the thin films or powders. Since the use of monolith might effectively reduce the high-
258 pressure drop, this would avoid adsorbent loss and secondary pollution during an adsorption
259 operation. Moreover, the monolith can be used in continuous flow microreactor instead of
260 conventional packed-bed reactors [62,63]. The HPCM showed the combined properties of

261 both mesoporous HPC (i.e., high specific surface area, uniform pore size, large pore volume,
262 interconnected pore channels for adsorption, good chemical inertness and stability), and
263 macroporous HPC (i.e., mass transport, fast accessibility of the bulky reagents/adsorbates and
264 high storage capacity) [52,63–65].

265

266 **4. Engineered HPCs**

267 Additional micropores and mesopores can be developed through HPC modification, and it
268 enhances the adsorption of organic contaminants [66]. Some strategies as explained in the
269 previous sections have been recommended to synthesize HPCs, and a combination of
270 template carbonization and chemical activation might improve the porous structure
271 development in HPCs (Figure 3). Generally, it includes two steps. Firstly, carbon materials
272 incorporated with hard templates (e.g., silica, nano-CaCO₃, nano-MgO, nano-Fe₂O₃, and
273 nano-ZnO) are carbonized at high temperature under an inert atmosphere. This process
274 creates meso- and macropores. Secondly, chemical activation (i.e., KOH or NaOH) is used to
275 develop the micropores [67]. The SSA of HPCs following template carbonization and
276 chemical activation can reach beyond 2000 m² g⁻¹, and generally comprises micropores of >2
277 nm size [68].

278 Yu et al. [67] studied the production of HPCs activated by KOH, having different
279 concentrations (i.e., 1, 2 and 3 M). Enteromorpha, a sea weed, was used as the precursor for
280 the synthesis of HPCs. Contrasting to the conventional activation of carbonized materials,
281 carbonization and chemical activation were simultaneously carried out at 800 °C. The
282 scanning electron microscopy (SEM) images showed the development of highly porous
283 HPCs with interconnected macropores (i.e., 200-1000 nm) with an increase of KOH

284 concentration. Moreover, X-ray photoelectron spectroscopy (XPS) analysis indicated the
285 considerably high heteroatom (i.e., N and O) doping in HPCs.

286 Hu et al. [68] developed a new method by coupling the *in situ* template with a NaOH
287 activation to enhance the porous structure of HPCs. They used lotus seed shell as the biomass
288 and sodium phytate as the hard template precursor. During the carbonization, sodium phytate
289 converted to nano- $\text{Na}_5\text{P}_3\text{O}_{10}$ and reacted with NaOH. During this reaction, nano- Na_2CO_3 and
290 nano- Na_3PO_4 particles were generated and homogeneously dispersed in the biomass creating
291 large mesopores and macropores after washing with HCl. Moreover, NaOH created
292 micropores, and ultimately produced a well-developed hollow nest-like structure of HPC. It
293 showed very high SSA of $3188 \text{ m}^2 \text{ g}^{-1}$ and total pore volume of $3.2 \text{ cm}^3 \text{ g}^{-1}$. Conventional
294 NaOH activation is well known to produce micropores. However, the authors clearly showed
295 that NaOH activation with the addition of sodium phytate could create HPCs with micro-,
296 meso- and macropores. Similarly, Chen et al. [69] carried out carbonization and chemical
297 activation by KOH concurrently, and developed HPCs with high micro-, meso- and macro-
298 pores. They were able to produce N self-doped 3D porous HPCs from waste cottonseed husk
299 by a one-step chemical activation.

300 A hydrochar material produced from eucalyptus sawdust was chemically activated by the
301 mixture of potassium oxalate monohydrate ($\text{K}_2\text{C}_2\text{O}_4$) and powdered melamine ($\text{C}_3\text{H}_6\text{N}_6$) to
302 enhance the porous structure [70]. Authors reported the presence of randomly distributed
303 pores in HPCs via high-resolution transmission electron microscopic observations. Moreover,
304 the XRD and Raman spectroscopy analyses revealed the presence of amorphous-like
305 structure. Nitrogen adsorption-desorption isotherms results of HPCs showed an enlargement
306 of pore size corresponding to increased melamine/hydrochar ratio, however, HPCs had >70%

307 of micro pore volume from total pore volume. The optimum activation of hydrochar by
308 $K_2C_2O_4$ and $C_3H_6N_6$ (i.e., $K_2C_2O_4$ /hydrochar = 3.6–6 and $C_3H_6N_6$ /hydrochar = 2) generated
309 HPC showed $3000\text{ m}^2\text{ g}^{-1}$ of SSA which was similar to HPC obtained under harsh KOH
310 activation conditions [71,72]. Hence, $K_2C_2O_4$ and $C_3H_6N_6$ can be substituted as promising
311 chemicals instead of KOH to improve the porous structure of HPCs. In addition, these two
312 chemicals are less corrosive compared to the KOH, causing less technical constraints [70].

313 The HPCs produced with synthetic carbon precursors are also modified with different
314 chemicals. For instance, Wu et al. [73] produced HPCs with o-phenylenediamine and
315 modified with ammonium persulfate ($(NH_4)_2S_2O_8$), and potassium ferricyanide
316 ($K_3[Fe(CN)_6]$) to create Fe active sites, and N and S doping in HPCs. Authors did the
317 carbonization and chemical modification simultaneously at $600\text{ }^\circ\text{C}$ for 3 h after several
318 sample preparation steps. Scanning transmission electron microscopy (STEM) coupled with
319 energy-dispersive spectroscopy (EDS) clearly visualized the doping of Fe, N and S in HPCs.

320 Górká and Jaroniec [74] produced different HPCs using polymeric carbon precursors and
321 block copolymer template in acidic conditions with tetraethyl orthosilicate (TEOS) and
322 colloidal silica. They developed cylindrical and spherical mesopores having dimensions of 12
323 nm and 20-50 nm, respectively. The thermal decomposition of the soft template created the
324 cylindrical mesopores, dissolution of colloidal silica resulted the spherical mesopores, and the
325 dissolution of TEOS created the fine pores in HPCs. In addition, post activation of HPCs with
326 carbon dioxide and water vapour further increased the fine pores, and the surface area
327 increased up to $2800\text{ m}^2\text{ g}^{-1}$. Similarly, Lee et al. [75] synthesized HPCs with high surface
328 area (i.e., $1625\text{--}1796\text{ m}^2\text{ g}^{-1}$) and porosity from polyacrylonitrile fibers, silica template, and

329 via post activation of KOH. They developed a porous structure with < 2 nm micropores, 2-5
330 and 10-50 nm mesopores, and > 50 nm macropores.

331

332 **5. Removal of aqueous organic contaminants by HPCs and associated mechanisms**

333 In recent years, with the advancement of industrial activities, organic contaminants
334 including dyes, pharmaceuticals, pesticides, hydrocarbons and other emerging contaminants
335 are being continuously released into the aquatic environment, and causing the environmental
336 problems, which ultimately affect humans' health. To control and limit the impact of organic
337 contaminants on the environment and human health, the urge for exploring novel adsorbents
338 with excellent adsorption performance to remove the pollutants from contaminated water is
339 growing steadily (Table 2).

340 Traditionally, activated carbons have played an important role in the adsorption field
341 because of their very high SSA and porosities. Activated carbons, however, suffer from
342 limitations, such as the limited interconnectivity between defective and irregular microporous
343 structures that restricts the contaminant molecule's access to the adsorbent surface. Ji et al.
344 [76] found that the pore structure of template-synthesized carbon adsorbent primarily
345 supported the adsorption of antibiotics (i.e., sulfamethoxazole, tetracycline, and tylosin),
346 while the highly disordered and closed pore structure of activated carbons may lead to the
347 size-exclusion effect or slow adsorption kinetics. Therefore, it is necessary to use the
348 templating method to synthesize carbon materials to make up the structural weakness of
349 activated carbons and promote the adsorption performance of the carbon materials.

350 Nowadays, HPCs possessing uniform macropores and interconnected meso- and/or
351 micropores for adsorption have received considerable research attention. This is mainly

352 because of the unique properties of HPCs such as fine and well-defined pore systems,
353 excellent performance of mass transport via larger pores, and the high amount of adsorption
354 sites at smaller pores. There are only few reports about the adsorption of organic
355 contaminants by HPCs, and the studied organic contaminants included dyes (methylene blue),
356 antibiotics (sulfamethazin, tetracycline, chloramphenicol), hydrocarbons (phenol, bisphenol
357 A), oil, bilirubin, etc. The molecular size of the studied organic contaminants was diverse
358 including bulky (e.g., oil, bilirubin, dyes) as well as small (e.g., antibiotic, hydrocarbon)
359 molecules, which showed the extensive application potentials of HPCs in the field of
360 contaminant adsorption.

361 The HPC monoliths (HPCMs) with three-dimensionally connected macroporous and
362 ordered hexagonal mesoporous structures were developed via an optimized hydrothermal
363 process followed by a nanocasting pathway [63]. Because of strong hydrophobicity (water
364 contact angle at $140 \pm 3^\circ$) and extremely low density ($0.017 \pm 0.002 \text{ g cm}^{-3}$), HPCMs
365 performed as a superior adsorbent compared with conventional mesoporous carbon CMK-3
366 and traditional activated carbon. The oil adsorption capacity of HPCMs reached to 45 mg g^{-1}
367 within a few seconds. The extraordinarily high SSA ($1354 \text{ m}^2 \text{ g}^{-1}$), macroporous cumulative
368 volume ($48.6 \text{ cm}^3 \text{ g}^{-1}$), and ordered mesoporous and 3D connected microporous structures
369 contributed to the high rate of oil adsorption by the material. In addition, bilirubin adsorption
370 on HPCMs took place within 2 h, accounting for 86.8% removal (equilibrium concentration =
371 700 mg L^{-1}). The bilirubin adsorption capacity of HPCMs was 613 mg g^{-1} , which was
372 remarkably higher than single mesoporous or microporous carbon materials [63].

373 Liu et al. (2012) developed a macro-meso-micro HPC using two types of diatomites (i.e.,
374 Dt(JL) and Dt(SD) as the template and catalyst) for methylene blue (MB) adsorption. The

375 structure of the HPC was dependent on the original form of the template, and the SSA of the
376 templated carbon materials was $270 \text{ m}^2 \text{ g}^{-1}$ and $335 \text{ m}^2 \text{ g}^{-1}$, respectively. Within 20 min, the
377 adsorption of MB on both the diatomite-templated carbon materials reached the equilibrium
378 state, showing a fast adsorption process. The maximum monolayer adsorption capacity (Q_m)
379 values of the template materials were 333 mg g^{-1} and 250 mg g^{-1} , respectively, indicating a
380 higher adsorption capacity than commercial activated carbon (CAC) [77].

381 Dai et al. [78] reported adsorptive removal of sulfamethazine by lignin-based HPCs with 3-
382 D interconnected macroporous and meso-/microporous structures. The meso-/micropores
383 produced by the activation of KOH was less than 4 nm in diameter, and the macropore
384 diameter was about 200 nm. The Q_m of sulfamethazine by the HPC was 869.6 mg g^{-1} at 308
385 K. The strong adsorption affinity of the HPC to sulfamethazine was due to its high SSA (2784
386 $\text{m}^2 \text{ g}^{-1}$) and pore volume ($1.382 \text{ cm}^3 \text{ g}^{-1}$). Owing to the well-defined 3-D interconnected
387 hierarchical porous structure, the adsorption kinetics of the HPC was fast in the first 30 min
388 [79]. The same research group used carbon nanotubes as hard templates to synthesize HPCs,
389 which had excellent adsorption capacities for chloramphenicol and tetracycline (1297 mg g^{-1}
390 and 1067.2 mg g^{-1} , respectively), far higher than previously reported values. The sample had
391 a wide pore size distribution, ranging from < 2 to 100 nm [80].

392 Tripathi et al. [81] reported bisphenol A (BPA) removal by hierarchically ordered micro-
393 mesoporous carbon with an ultra-high adsorption capacity of 1106 mg g^{-1} , which is three
394 times larger than that activated carbons of a previous study of Liu et al. [82]. In particular, the
395 sizes of the micropores and mesopores were tailored and enlarged to 1.3 nm and 9.0 nm,
396 respectively, to accommodate the molecular dimensions of BPA for achieving an optimal
397 adsorption performance. This was achieved by controlling the condensation behavior of

398 phloroglucinol-terephthalaldehyde resin. Besides, kinetic studies revealed that the mesopores
399 were the key to promote adsorbate diffusion through the pore channels, and the smaller
400 secondary micropores contributed to the high adsorption capacity, achieving a removal rate of
401 86% (743 mg g^{-1}), which was higher than that of the single mesoporous material. The authors
402 demonstrated that controlling the porosity and structural features of ordered carbon materials
403 were effective to promote the adsorption of BPA [81].

404 In order to explore the effect of porosities (of all sizes) and to demonstrate the relative role
405 of each pore size class on the adsorption process in a liquid media, Bulavová et al. [83]
406 prepared single microporous, micro-mesoporous and micro-meso-macroporous carbon
407 materials by changing the synthesis conditions. Methylene blue and phenol (molecular
408 diameters vary greatly; 1.3 nm and 0.75 nm, respectively) were chosen as molecular probes
409 for testing the adsorbents. Both adsorption rate and adsorption capacity of micro-mesoporous
410 carbon were far more favorable than those of the single microporous carbon. Meanwhile, the
411 presence of macropores further promoted the adsorption. The functional groups of
412 micropores were different from those of the micro-mesoporous and micro-meso-macroporous
413 carbons. However, the authors suggested that the functional groups were not the decisive
414 factor for adsorption because the diffusion restriction posed by the microporous system made
415 it impossible for the adsorbates to reach the adsorbent active sites [83].

416 For the adsorption of super-large molecules (e.g., gasoline), it is important to mention that
417 the macropore volume/mesopore volume needs to be relatively high. It is reasonable to
418 consider that macropores play a predominant role in adsorbing capacious gasoline, while
419 mesopores can induce roughness on the surface of the macropores and high surface area,

420 which can benefit the dispersive interactions between carbon basal planes and the adsorbate
421 [63].

422 The analysis of adsorption mechanisms of sulfamethazine antibiotics showed higher
423 adsorption capacities of HPCs, which might be attributed to its high SSA (i.e., 2784 m² g⁻¹)
424 and large pore volume (i.e., 1.382 cm³ g⁻¹). In addition, the van der Waals forces between the
425 antibiotic molecules and the adsorbent, and the π - π electron-donor-acceptor interactions of
426 the antibiotic molecules at the plane of benzene rings might also affect the adsorption [79].
427 Furthermore, hydrophilic antibiotics had a higher adsorption on the studied HPC, indicating
428 that the hydrophilic process promoted the adsorption capacity [80].

429

430 **6. Conclusions and future prospects**

431 HPCs are emerging adsorbents that can be promisingly applied for the removal of
432 organic pollutants from contaminated water. The highly porous structure and easily tunable
433 structural arrangements provide advantages in designing highly effective HPCs for organic
434 contaminants removal. Moreover, waste biomass such as crop residues, agricultural wastes
435 and food wastes can be used to produce HPCs, introducing an additional benefit of waste
436 management and low-cost. The use of HPCs in water treatment related studies has increased
437 just recently, but applications of these materials for treating organic contaminants in
438 wastewater are not yet at a satisfactory level. According to SCOPUS database, the first
439 publication on HPC application in removing aqueous organic contaminants appeared in 2012
440 [84]. Since then, there has been no extensive growth in this area of research. This might be
441 due to the strong focus of HPCs concerning super capacitor and energy storage applications.
442 Hence, there is a huge research scope in the use of HPCs for water remediation. Optimal and

443 effective HPC modification methods to enhance their ability to remove aqueous organic
444 contaminants are also not adequately available. Since HPCs are easily tunable, they have a
445 promising capacity to be used in commercial filtration materials, such as membranes and
446 filters for household and large-scale wastewater treatments. Hence, more research is essential
447 to improve and implement the HPCs for water remediation as an energy- and cost-
448 inexpensive technology.

449

450 **Acknowledgments**

451 The authors acknowledge the financial support from the National Natural Science
452 Foundations of China (21677137), “National Science and Technology Major Projects for
453 Water Pollution Control and Treatment (Grant No. 2017ZX07201004)”, and “Fundamental
454 Research Funds for the Central Universities (2019FZJD007)”.

455

456 **References**

- 457 [1] Fu R, Li Z, Liang Y, Li F, Xu F, Wu D. Hierarchical porous carbons: design,
458 preparation, and performance in energy storage. *New Carbon Mater* 2011;26:171–9.
459 [https://doi.org/10.1016/S1872-5805\(11\)60074-7](https://doi.org/10.1016/S1872-5805(11)60074-7).
- 460 [2] Yang Z, Ren J, Zhang Z, Chen X, Guan G, Qiu L, et al. Recent Advancement of
461 Nanostructured Carbon for Energy Applications. *Chem Rev* 2015;115:5159–223.
462 <https://doi.org/10.1021/cr5006217>.
- 463 [3] Gao M, Shih C-C, Pan S-Y, Chueh C-C, Chen W-C. Advances and challenges of green
464 materials for electronics and energy storage applications: from design to end-of-life
465 recovery. *J Mater Chem A* 2018;6:20546–63. <https://doi.org/10.1039/C8TA07246A>.

- 466 [4] Liu F, Wang Z, Zhang H, Jin L, Chu X, Gu B, et al. Nitrogen, oxygen and sulfur co-
467 doped hierarchical porous carbons toward high-performance supercapacitors by direct
468 pyrolysis of kraft lignin. *Carbon N Y* 2019;149:105–16.
469 <https://doi.org/10.1016/J.CARBON.2019.04.023>.
- 470 [5] Sun M, Wang X, Pan X, Liu L, Li Y, Zhao Z, et al. Nitrogen-rich hierarchical porous
471 carbon nanofibers for selective oxidation of hydrogen sulfide. *Fuel Process Technol*
472 2019;191:121–8. <https://doi.org/10.1016/J.FUPROC.2019.03.020>.
- 473 [6] Li Z, Gao S, Mi H, Lei C, Ji C, Xie Z, et al. High-energy quasi-solid-state
474 supercapacitors enabled by carbon nanofoam from biowaste and high-voltage
475 inorganic gel electrolyte. *Carbon N Y* 2019;149:273–80.
476 <https://doi.org/10.1016/J.CARBON.2019.04.056>.
- 477 [7] Liu H, Wei Y, Luo J, Li T, Wang D, Luo S, et al. 3D hierarchical porous-structured
478 biochar aerogel for rapid and efficient phenicol antibiotics removal from water. *Chem*
479 *Eng J* 2019;368:639–48. <https://doi.org/10.1016/J.CEJ.2019.03.007>.
- 480 [8] Xu F, Han H, Ding B, Qiu Y, Zhang E, Li H, et al. Engineering pore ratio in
481 hierarchical porous carbons towards high-rate and large-volumetric performances.
482 *Microporous Mesoporous Mater* 2019;282:205–10.
483 <https://doi.org/10.1016/J.MICROMESO.2019.03.038>.
- 484 [9] Paraknowitsch JP, Thomas A. Doping carbons beyond nitrogen: an overview of
485 advanced heteroatom doped carbons with boron, sulphur and phosphorus for energy
486 applications. *Energy Environ Sci* 2013;6:2839. <https://doi.org/10.1039/c3ee41444b>.
- 487 [10] Sun J-K, Xu Q. Functional materials derived from open framework
488 templates/precursors: synthesis and applications. *Energy Environ Sci* 2014;7:2071.

- 489 <https://doi.org/10.1039/c4ee00517a>.
- 490 [11] Xu D, Tong Y, Yan T, Shi L, Zhang D. N,P-Codoped Meso-/Microporous Carbon
491 Derived from Biomass Materials via a Dual-Activation Strategy as High-Performance
492 Electrodes for Deionization Capacitors. *ACS Sustain Chem Eng* 2017;5:5810–9.
493 <https://doi.org/10.1021/acssuschemeng.7b00551>.
- 494 [12] Béguin F, Presser V, Balducci A, Frackowiak E. Carbons and Electrolytes for
495 Advanced Supercapacitors. *Adv Mater* 2014;26:2219–51.
496 <https://doi.org/10.1002/adma.201304137>.
- 497 [13] Wang Q, Yan J, Fan Z. Carbon materials for high volumetric performance
498 supercapacitors: design, progress, challenges and opportunities. *Energy Environ Sci*
499 2016;9:729–62. <https://doi.org/10.1039/C5EE03109E>.
- 500 [14] Zheng X, Luo J, Lv W, Wang D-W, Yang Q-H. Two-Dimensional Porous Carbon:
501 Synthesis and Ion-Transport Properties. *Adv Mater* 2015;27:5388–95.
502 <https://doi.org/10.1002/adma.201501452>.
- 503 [15] Ok YS, Chang SX, Gao B, Chung HJ. SMART biochar technology-A shifting
504 paradigm towards advanced materials and healthcare research. *Environ Technol Innov*
505 2015;4:206–9. <https://doi.org/10.1016/j.eti.2015.08.003>.
- 506 [16] Igalavithana AD, Mandal S, Niazi NK, Vithanage M, Parikh SJ, Mukome FND, et al.
507 Advances and future directions of biochar characterization methods and applications.
508 *Crit Rev Environ Sci Technol* 2017;47:2275–330.
509 <https://doi.org/10.1080/10643389.2017.1421844>.
- 510 [17] Mohan D, Sarswat A, Ok YS, Pittman CU. Organic and inorganic contaminants
511 removal from water with biochar, a renewable, low cost and sustainable adsorbent – A

- 512 critical review. *Bioresour Technol* 2014;160:191–202.
- 513 <https://doi.org/10.1016/j.biortech.2014.01.120>.
- 514 [18] Tran NH, Reinhard M, Khan E, Chen H, Nguyen VT, Li Y, et al. Emerging
515 contaminants in wastewater, stormwater runoff, and surface water: Application as
516 chemical markers for diffuse sources. *Sci Total Environ* 2019;676:252–67.
517 <https://doi.org/10.1016/J.SCITOTENV.2019.04.160>.
- 518 [19] Fu J, Lee W-N, Coleman C, Nowack K, Carter J, Huang C-H. Removal of
519 pharmaceuticals and personal care products by two-stage biofiltration for drinking
520 water treatment. *Sci Total Environ* 2019;664:240–8.
521 <https://doi.org/10.1016/J.SCITOTENV.2019.02.026>.
- 522 [20] Ebele AJ, Abou-Elwafa Abdallah M, Harrad S. Pharmaceuticals and personal care
523 products (PPCPs) in the freshwater aquatic environment. *Emerg Contam* 2017;3:1–16.
524 <https://doi.org/10.1016/J.EMCON.2016.12.004>.
- 525 [21] Yang Y, Ok YS, Kim K-H, Kwon EE, Tsang YF. Occurrences and removal of
526 pharmaceuticals and personal care products (PPCPs) in drinking water and
527 water/sewage treatment plants: A review. *Sci Total Environ* 2017;596–597:303–20.
528 <https://doi.org/10.1016/J.SCITOTENV.2017.04.102>.
- 529 [22] Rajapaksha AU, Vithanage M, Ahmad M, Seo DC, Cho JS, Lee SE, et al. Enhanced
530 sulfamethazine removal by steam-activated invasive plant-derived biochar. *J Hazard*
531 *Mater* 2015;290:43–50. <https://doi.org/10.1016/j.jhazmat.2015.02.046>.
- 532 [23] Vithanage M, Rajapaksha AU, Tang X, Thiele-Bruhn S, Kim KH, Lee S-E, et al.
533 Sorption and transport of sulfamethazine in agricultural soils amended with invasive-
534 plant-derived biochar. *J Environ Manage* 2014;141:95–103.

- 535 <https://doi.org/10.1016/j.jenvman.2014.02.030>.
- 536 [24] Awad YM, Kim S-C, Abd El-Azeem SAM, Kim K-H, Kim K-R, Kim K, et al.
537 Veterinary antibiotics contamination in water, sediment, and soil near a swine manure
538 composting facility. *Environ Earth Sci* 2014;71:1433–40.
539 <https://doi.org/10.1007/s12665-013-2548-z>.
- 540 [25] Tian W, Zhang H, Duan X, Sun H, Tade MO, Ang HM, et al. Nitrogen- and Sulfur-
541 Codoped Hierarchically Porous Carbon for Adsorptive and Oxidative Removal of
542 Pharmaceutical Contaminants. *ACS Appl Mater Interfaces* 2016;8:7184–93.
543 <https://doi.org/10.1021/acsami.6b01748>.
- 544 [26] Rajapaksha AU, Alam MS, Chen N, Alessi DS, Igalavithana AD, Tsang DCW, et al.
545 Removal of hexavalent chromium in aqueous solutions using biochar: Chemical and
546 spectroscopic investigations. *Sci Total Environ* 2018;625:1567–73.
547 <https://doi.org/10.1016/J.SCITOTENV.2017.12.195>.
- 548 [27] Wu Y, Xia Y, Jing X, Cai P, Igalavithana AD, Tang C, et al. Recent advances in
549 mitigating membrane biofouling using carbon-based materials. *J Hazard Mater*
550 2020;382:120976. <https://doi.org/10.1016/J.JHAZMAT.2019.120976>.
- 551 [28] Wang S, Zhao M, Zhou M, Li YC, Wang J, Gao B, et al. Biochar-supported nZVI
552 (nZVI/BC) for contaminant removal from soil and water: A critical review. *J Hazard*
553 *Mater* 2019;373:820–34. <https://doi.org/10.1016/J.JHAZMAT.2019.03.080>.
- 554 [29] Yuan Z-Y, Su B-L. Insights into hierarchically meso–macroporous structured
555 materials. *J Mater Chem* 2006;16:663–77. <https://doi.org/10.1039/B512304F>.
- 556 [30] Kaur P, Verma G, Sekhon SS. Biomass derived hierarchical porous carbon materials
557 as oxygen reduction reaction electrocatalysts in fuel cells. *Prog Mater Sci* 2019;102:1–

- 558 71. <https://doi.org/10.1016/j.pmatsci.2018.12.002>.
- 559 [31] Guo T, Gao J, Xu M, Ju Y, Li J, Xue H. Hierarchically Porous Organic Materials
560 Derived From Copolymers: Preparation and Electrochemical Applications. *Polym Rev*
561 2019;59:149–86. <https://doi.org/10.1080/15583724.2018.1488730>.
- 562 [32] Liu YN, Zhang JN, Wang HT, Kang XH, Bian SW. Boosting the electrochemical
563 performance of carbon cloth negative electrodes by constructing hierarchically porous
564 nitrogen-doped carbon nanofiber layers for all-solid-state asymmetric supercapacitors.
565 *Mater Chem Front* 2019;3:25–31. <https://doi.org/10.1039/c8qm00293b>.
- 566 [33] Knox JH, Kaur B, Millward GR. Structure and performance of porous graphitic carbon
567 in liquid chromatography. *J Chromatogr A* 1986;352:3–25.
568 [https://doi.org/10.1016/S0021-9673\(01\)83368-9](https://doi.org/10.1016/S0021-9673(01)83368-9).
- 569 [34] Wang Y, Tao S, An Y. Superwetting monolithic carbon with hierarchical structure as
570 supercapacitor materials. *Microporous Mesoporous Mater* 2012;163:249–58.
571 <https://doi.org/10.1016/J.MICROMESO.2012.07.044>.
- 572 [35] Chen A, Yu Y, Li Y, Wang Y, Li Y, Li S, et al. Synthesis of macro-mesoporous
573 carbon materials and hollow core/mesoporous shell carbon spheres as supercapacitors.
574 *J Mater Sci* 2016;51:4601–8. <https://doi.org/10.1007/s10853-016-9774-1>.
- 575 [36] Yonghui D, Chong L, Ting Y, Feng L, Fuqiang Z, Wan Y, et al. Facile Synthesis of
576 Hierarchically Porous Carbons from Dual Colloidal Crystal/Block Copolymer
577 Template Approach. *Chem Mater* 2007;19:3271–7.
578 <https://doi.org/10.1021/CM070600Y>.
- 579 [37] Zhang Y, Che E, Zhang M, Sun B, Gao J, Han J, et al. Increasing the dissolution rate
580 and oral bioavailability of the poorly water-soluble drug valsartan using novel

- 581 hierarchical porous carbon monoliths. *Int J Pharm* 2014;473:375–83.
582 <https://doi.org/10.1016/J.IJPHARM.2014.07.024>.
- 583 [38] Li N, Zheng M, Feng S, Lu H, Zhao B, Zheng J, et al. Fabrication of Hierarchical
584 Macroporous/Mesoporous Carbons via the Dual-Template Method and the Restriction
585 Effect of Hard Template on Shrinkage of Mesoporous Polymers. *J Phys Chem C*
586 2013;117:8784–92. <https://doi.org/10.1021/jp3127219>.
- 587 [39] Zhao Y, Zheng M, Cao J, Ke X, Liu J, Chen Y, et al. Easy synthesis of ordered
588 meso/macroporous carbon monolith for use as electrode in electrochemical capacitors.
589 *Mater Lett* 2008;62:548–51. <https://doi.org/10.1016/J.MATLET.2007.06.002>.
- 590 [40] Zhu H, Liu Z, Wang Y, Kong D, Yuan X, Xie Z. Nanosized CaCO₃ as hard template
591 for creation of intracrystal pores within silicalite-1 crystal. *Chem Mater* 2008;20:1134–
592 9. <https://doi.org/10.1021/cm071385o>.
- 593 [41] Ilnicka A, Lukaszewicz JP. Synthesis of N-rich microporous carbon materials from
594 chitosan by alkali activation using Na₂CO₃. *Mater Sci Eng B Solid-State Mater Adv*
595 *Technol* 2015;201:66–71. <https://doi.org/10.1016/j.mseb.2015.08.002>.
- 596 [42] Song Y, Li W, Xu Z, Ma C, Liu Y, Xu M, et al. Hierarchical porous carbon spheres
597 derived from larch sawdust via spray pyrolysis and soft-templating method for
598 supercapacitors. *SN Appl Sci* 2019;1:122. <https://doi.org/10.1007/s42452-018-0132-6>.
- 599 [43] Liang Z, Zhang L, Liu H, Zeng J, Zhou J, Li H, et al. Soft-template assisted
600 hydrothermal synthesis of size-tunable, N-doped porous carbon spheres for
601 supercapacitor electrodes. *Results Phys* 2019;12:1984–90.
602 <https://doi.org/10.1016/J.RINP.2019.01.074>.
- 603 [44] Chai GS, Shin IS, Yu J-S. Synthesis of Ordered, Uniform, Macroporous Carbons with

- 604 Mesoporous Walls Templated by Aggregates of Polystyrene Spheres and Silica
605 Particles for Use as Catalyst Supports in Direct Methanol Fuel Cells. *Adv Mater*
606 2004;16:2057–61. <https://doi.org/10.1002/adma.200400283>.
- 607 [45] Woo S-W, Dokko K, Nakano H, Kanamura K. Preparation of three dimensionally
608 ordered macroporous carbon with mesoporous walls for electric double-layer
609 capacitors. *J Mater Chem* 2008;18:1674. <https://doi.org/10.1039/b717996k>.
- 610 [46] Seo J, Park H, Shin K, Baeck SH, Rhym Y, Shim SE. Lignin-derived macroporous
611 carbon foams prepared by using poly(methyl methacrylate) particles as the template.
612 *Carbon N Y* 2014;76:357–67. <https://doi.org/10.1016/j.carbon.2014.04.087>.
- 613 [47] Meng Y, Gu D, Zhang F, Shi Y, Yang H, Li Z, et al. Ordered Mesoporous Polymers
614 and Homologous Carbon Frameworks: Amphiphilic Surfactant Templating and Direct
615 Transformation. *Angew Chemie* 2005;117:7215–21.
616 <https://doi.org/10.1002/ange.200501561>.
- 617 [48] Ryoo R, Joo SH, Jun S. Synthesis of Highly Ordered Carbon Molecular Sieves via
618 Template-Mediated Structural Transformation 1999.
619 <https://doi.org/10.1021/JP991673A>.
- 620 [49] Li H, Yuan D, Tang C, Wang S, Sun J, Li Z, et al. Lignin-derived interconnected
621 hierarchical porous carbon monolith with large areal/volumetric capacitances for
622 supercapacitor. *Carbon N Y* 2016;100:151–7.
623 <https://doi.org/10.1016/J.CARBON.2015.12.075>.
- 624 [50] Zhang S, Chen L, Zhou S, Zhao D, Wu L. Facile Synthesis of Hierarchically Ordered
625 Porous Carbon via *in Situ* Self-Assembly of Colloidal Polymer and Silica Spheres and
626 Its Use as a Catalyst Support. *Chem Mater* 2010;22:3433–40.

- 627 <https://doi.org/10.1021/cm1002274>.
- 628 [51] Wang Z, Kiesel ER, Stein A. Silica-free syntheses of hierarchically ordered
629 macroporous polymer and carbon monoliths with controllable mesoporosity. *J Mater*
630 *Chem* 2008;18:2194. <https://doi.org/10.1039/b719489g>.
- 631 [52] Xue C, Tu B, Zhao D. Facile fabrication of hierarchically porous carbonaceous
632 monoliths with ordered mesostructure via an organic organic self-assembly. *Nano Res*
633 2009;2:242–53. <https://doi.org/10.1007/s12274-009-9022-y>.
- 634 [53] Huang C-H, Doong R-A. Sugarcane bagasse as the scaffold for mass production of
635 hierarchically porous carbon monoliths by surface self-assembly. *Microporous*
636 *Mesoporous Mater* 2012;147:47–52.
637 <https://doi.org/10.1016/J.MICROMESO.2011.05.027>.
- 638 [54] Chen W, Zhang H, Huang Y, Wang W. A fish scale based hierarchical lamellar porous
639 carbon material obtained using a natural template for high performance
640 electrochemical capacitors. *J Mater Chem* 2010;20:4773.
641 <https://doi.org/10.1039/c0jm00382d>.
- 642 [55] Gao A, Guo N, Yan M, Li M, Wang F, Yang R. Hierarchical porous carbon activated
643 by CaCO₃ from pigskin collagen for CO₂ and H₂ adsorption. *Microporous*
644 *Mesoporous Mater* 2018;260:172–9.
645 <https://doi.org/10.1016/J.MICROMESO.2017.08.048>.
- 646 [56] Vernimmen J, Meynen V, Cool P. Synthesis and catalytic applications of combined
647 zeolitic/mesoporous materials. *Beilstein J Nanotechnol* 2011;2:785–801.
648 <https://doi.org/10.3762/bjnano.2.87>.
- 649 [57] Xia K, Gao Q, Jiang J, Hu J. Hierarchical porous carbons with controlled micropores

650 and mesopores for supercapacitor electrode materials. *Carbon N Y* 2008;46:1718–26.
651 <https://doi.org/10.1016/J.CARBON.2008.07.018>.

652 [58] Yang G, Han H, Li T, Du C. Synthesis of nitrogen-doped porous graphitic carbons
653 using nano-CaCO₃ as template, graphitization catalyst, and activating agent. *Carbon N*
654 *Y* 2012;50:3753–65. <https://doi.org/10.1016/J.CARBON.2012.03.050>.

655 [59] Martín-Jimeno FJ, Suárez-García F, Paredes JI, Enterría M, Pereira MFR, Martins JI,
656 et al. A “Nanopore Lithography” Strategy for Synthesizing Hierarchically
657 Micro/Mesoporous Carbons from ZIF-8/Graphene Oxide Hybrids for Electrochemical
658 Energy Storage. *ACS Appl Mater Interfaces* 2017;9:44740–55.
659 <https://doi.org/10.1021/acsami.7b16567>.

660 [60] Siyasukh A, Maneeprom P, Larpkiattaworn S, Tonanon N, Tanthapanichakoon W,
661 Tamon H, et al. Preparation of a carbon monolith with hierarchical porous structure by
662 ultrasonic irradiation followed by carbonization, physical and chemical activation.
663 *Carbon N Y* 2008;46:1309–15. <https://doi.org/10.1016/J.CARBON.2008.05.006>.

664 [61] Zou C, Wu D, Li M, Zeng Q, Xu F, Huang Z, et al. Template-free fabrication of
665 hierarchical porous carbon by constructing carbonyl crosslinking bridges between
666 polystyrene chains. *J Mater Chem* 2010;20:731–5. <https://doi.org/10.1039/B917960G>.

667 [62] Lu A-H, Li W-C, Schmidt W, Schüth F. Fabrication of hierarchically structured carbon
668 monoliths via self-binding and salt templating. *Microporous Mesoporous Mater*
669 2006;95:187–92. <https://doi.org/10.1016/J.MICROMESO.2006.05.024>.

670 [63] Tao G, Zhang L, Hua Z, Chen Y, Guo L, Zhang J, et al. Highly efficient adsorbents
671 based on hierarchically macro/mesoporous carbon monoliths with strong
672 hydrophobicity. *Carbon N Y* 2014;66:547–59.

- 673 <https://doi.org/10.1016/J.CARBON.2013.09.037>.
- 674 [64] García A, Nieto A, Vila M, Vallet-Regí M. Easy synthesis of ordered mesoporous
675 carbon containing nickel nanoparticles by a low temperature hydrothermal method.
676 Carbon N Y 2013;51:410–8. <https://doi.org/10.1016/J.CARBON.2012.08.074>.
- 677 [65] Flexer V, Brun N, Destribats M, Backov R, Mano N. A novel three-dimensional
678 macrocellular carbonaceous biofuel cell. Phys Chem Chem Phys 2013;15:6437.
679 <https://doi.org/10.1039/c3cp50807b>.
- 680 [66] Borchardt L, Zhu Q-L, Casco ME, Berger R, Zhuang X, Kaskel S, et al. Toward a
681 molecular design of porous carbon materials. Mater Today 2017;20:592–610.
682 <https://doi.org/10.1016/J.MATTOD.2017.06.002>.
- 683 [67] Yu W, Wang H, Liu S, Mao N, Liu X, Shi J, et al. N, O-codoped hierarchical porous
684 carbons derived from algae for high-capacity supercapacitors and battery anodes. J
685 Mater Chem A 2016;4:5973–83. <https://doi.org/10.1039/C6TA01821A>.
- 686 [68] Hu L, Zhu Q, Wu Q, Li D, An Z, Xu B. Natural Biomass-Derived Hierarchical Porous
687 Carbon Synthesized by an in Situ Hard Template Coupled with NaOH Activation for
688 Ultrahigh Rate Supercapacitors 2018;7.
689 <https://doi.org/10.1021/acssuschemeng.8b02299>.
- 690 [69] Chen H, Wang G, Chen L, Dai B, Yu F. Three-Dimensional Honeycomb-Like Porous
691 Carbon with Both Interconnected Hierarchical Porosity and Nitrogen Self-Doping
692 from Cotton Seed Husk for Supercapacitor Electrode. Nanomaterials 2018;8:412.
693 <https://doi.org/10.3390/nano8060412>.
- 694 [70] Sevilla M, Ferrero GA, Fuertes AB. Beyond KOH activation for the synthesis of
695 superactivated carbons from hydrochar. Carbon N Y 2017;114:50–8.

- 696 <https://doi.org/10.1016/J.CARBON.2016.12.010>.
- 697 [71] Fuertes AB, Sevilla M. High-surface area carbons from renewable sources with a
698 bimodal micro-mesoporosity for high-performance ionic liquid-based supercapacitors.
699 Carbon N Y 2015;94:41–52. <https://doi.org/10.1016/J.CARBON.2015.06.028>.
- 700 [72] Sevilla M, Fuertes AB. Sustainable porous carbons with a superior performance for
701 CO₂ capture. Energy Environ Sci 2011;4:1765. <https://doi.org/10.1039/c0ee00784f>.
- 702 [73] Wu K, Chen X, Liu S, Pan Y, Cheong W-C, Zhu W, et al. Porphyrin-like Fe-N₄ sites
703 with sulfur adjustment on hierarchical porous carbon for different rate-determining
704 steps in oxygen reduction reaction. Nano Res 2018;11:6260–9.
705 <https://doi.org/10.1007/s12274-018-2149-y>.
- 706 [74] Górka J, Jaroniec M. Hierarchically porous phenolic resin-based carbons obtained by
707 block copolymer-colloidal silica templating and post-synthesis activation with carbon
708 dioxide and water vapor. Carbon N Y 2011;49:154–60.
709 <https://doi.org/10.1016/J.CARBON.2010.08.055>.
- 710 [75] Lee D, Jung J-Y, Jung M-J, Lee Y-S. Hierarchical porous carbon fibers prepared using
711 a SiO₂ template for high-performance EDLCs. Chem Eng J 2015;263:62–70.
712 <https://doi.org/10.1016/J.CEJ.2014.10.070>.
- 713 [76] Ji L, Liu F, Xu Z, Zheng S, Zhu D. Adsorption of Pharmaceutical Antibiotics on
714 Template-Synthesized Ordered Micro- and Mesoporous Carbons. Environ Sci Technol
715 2010;44:3116–22. <https://doi.org/10.1021/es903716s>.
- 716 [77] Liu D, Yuan P, Tan D, Liu H, Wang T, Fan M, et al. Facile preparation of
717 hierarchically porous carbon using diatomite as both template and catalyst and
718 methylene blue adsorption of carbon products. J Colloid Interface Sci 2012;388:176–

- 719 84. <https://doi.org/10.1016/j.jcis.2012.08.023>.
- 720 [78] Dai J, Qin L, Zhang R, Xie A, Chang Z, Tian S, et al. Sustainable bovine bone-derived
721 hierarchically porous carbons with excellent adsorption of antibiotics: Equilibrium,
722 kinetic and thermodynamic investigation. *Powder Technol* 2018;331:162–70.
723 <https://doi.org/10.1016/J.POWTEC.2018.03.005>.
- 724 [79] Chang Z, Dai J, Xie A, He J, Zhang R, Tian S, et al. From Lignin to Three-
725 Dimensional Interconnected Hierarchically Porous Carbon with High Surface Area for
726 Fast and Superhigh-Efficiency Adsorption of Sulfamethazine. *Ind Eng Chem Res*
727 2017;56:9367–75. <https://doi.org/10.1021/acs.iecr.7b02312>.
- 728 [80] Xie A, Dai J, Chen X, Ma P, He J, Li C, et al. Ultrahigh adsorption of typical
729 antibiotics onto novel hierarchical porous carbons derived from renewable lignin via
730 halloysite nanotubes-template and in-situ activation. *Chem Eng J* 2016;304:609–20.
731 <https://doi.org/10.1016/J.CEJ.2016.06.138>.
- 732 [81] Tripathi PK, Liu M, Zhao Y, Ma X, Gan L, Noonan O, et al. Enlargement of uniform
733 micropores in hierarchically ordered micro–mesoporous carbon for high level
734 decontamination of bisphenol A. *J Mater Chem A* 2014;2:8534.
735 <https://doi.org/10.1039/c4ta00578c>.
- 736 [82] Liu G, Ma J, Li X, Qin Q. Adsorption of bisphenol A from aqueous solution onto
737 activated carbons with different modification treatments. *J Hazard Mater*
738 2009;164:1275–80. <https://doi.org/10.1016/J.JHAZMAT.2008.09.038>.
- 739 [83] Bulavová P, Parmentier J, Slovák V. Facile synthesis of soft-templated carbon
740 monoliths with hierarchical porosity for fast adsorption from liquid media.
741 *Microporous Mesoporous Mater* 2018;272:155–65.

- 742 <https://doi.org/10.1016/J.MICROMESO.2018.06.024>.
- 743 [84] Si Y, Ren T, Li Y, Ding B, Yu J. Fabrication of magnetic polybenzoxazine-based
744 carbon nanofibers with Fe₃O₄ inclusions with a hierarchical porous structure for water
745 treatment. *Carbon N Y* 2012;50:5176–85.
746 <https://doi.org/10.1016/J.CARBON.2012.06.059>.
- 747 [85] Liu H, Cao C-Y, Wei F-F, Jiang Y, Sun Y-B, Huang P-P, et al. Fabrication of
748 Macroporous/Mesoporous Carbon Nanofiber Using CaCO₃ Nanoparticles as Dual
749 Purpose Template and Its Application as Catalyst Support. *J Phys Chem C*
750 2013;117:21426–32. <https://doi.org/10.1021/jp4078807>.
- 751 [86] Yang D, Jing H, Wang Z, Li J, Hu M, Lv R, et al. Coupled ultrasonication-milling
752 synthesis of hierarchically porous carbon for high-performance supercapacitor. *J*
753 *Colloid Interface Sci* 2018;528:208–24. <https://doi.org/10.1016/J.JCIS.2018.05.050>.
- 754 [87] Li Z, Hu X, Xiong D, Li B, Wang H, Li Q. Facile synthesis of bicontinuous
755 microporous/mesoporous carbon foam with ultrahigh specific surface area for
756 supercapacitor application. *Electrochim Acta* 2016;219:339–49.
757 <https://doi.org/10.1016/J.ELECTACTA.2016.10.028>.
- 758 [88] Juhl AC, Elverfeldt C-P, Hoffmann F, Fröba M. Porous carbon monoliths with pore
759 sizes adjustable between 10 nm and 2 μm prepared by phase separation – New insights
760 in the relation between synthesis composition and resulting structure. *Microporous*
761 *Mesoporous Mater* 2018;255:271–80.
762 <https://doi.org/10.1016/J.MICROMESO.2017.07.040>.
- 763 [89] Baumann TF, Worsley MA, Han TY-J, Satcher JH. High surface area carbon aerogel
764 monoliths with hierarchical porosity. *J Non Cryst Solids* 2008;354:3513–5.

- 765 <https://doi.org/10.1016/J.JNONCRY SOL.2008.03.006>.
- 766 [90] Wang DW, Li F, Lu GQ, Cheng HM. Synthesis and dye separation performance of
767 ferromagnetic hierarchical porous carbon. *Carbon N Y* 2008;46:1593–9.
768 <https://doi.org/10.1016/J.CARBON.2008.06.052>.
- 769 [91] Li J, Bai H, Li X, Li W, Zhai J, Li M, et al. Hierarchical porous carbon microspheres
770 with superhydrophilic surface for efficient adsorption and detection of water-soluble
771 contaminants. *J Mater Chem A* 2018;6:12153–61.
772 <https://doi.org/10.1039/C8TA02143K>.
- 773 [92] Zhu Z, Ji C, Zhong L, Liu S, Cui F, Sun H, et al. Magnetic Fe–Co crystal doped
774 hierarchical porous carbon fibers for removal of organic pollutants. *J Mater Chem A*
775 2017;5:18071–80. <https://doi.org/10.1039/C7TA03990E>.
- 776 [93] Hu J, Noked M, Gillette E, Han F, Gui Z, Wang C, et al. Dual-template synthesis of
777 ordered mesoporous carbon/Fe₂O₃ nanowires: high porosity and structural stability
778 for supercapacitors. *J Mater Chem A* 2015;3:21501–10.
779 <https://doi.org/10.1039/C5TA06372H>.
- 780 [94] Lee J, Kim J, Hyeon T. Recent Progress in the Synthesis of Porous Carbon Materials.
781 *Adv Mater* 2006;18:2073–94. <https://doi.org/10.1002/adma.200501576>.
- 782 [95] Wu X, Lam CWK, Wu N, Pang S-S, Xing Z, Zhang W, et al. Multiple templates
783 fabrication of hierarchical porous carbon for enhanced rate capability in potassium-ion
784 batteries. *Mater Today Energy* 2019;11:182–91.
785 <https://doi.org/10.1016/J.MTENER.2018.11.009>.
- 786 [96] Guo N, Li M, Sun X, Wang F, Yang R. Enzymatic hydrolysis lignin derived
787 hierarchical porous carbon for supercapacitors in ionic liquids with high power and

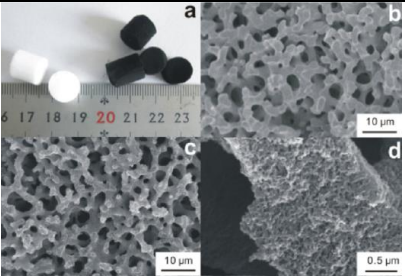
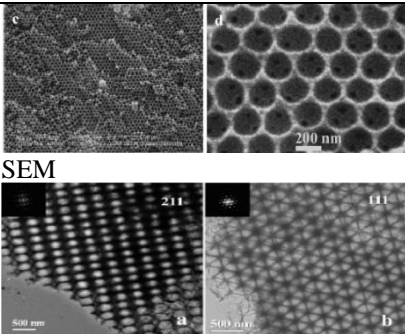
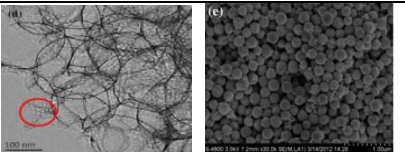
788 energy densities. *Green Chem* 2017;19:2595–602.
789 <https://doi.org/10.1039/C7GC00506G>.

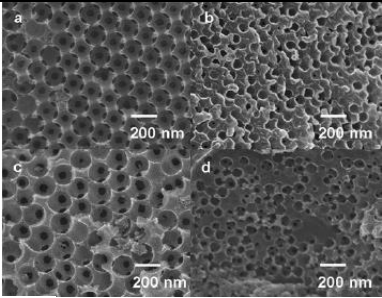
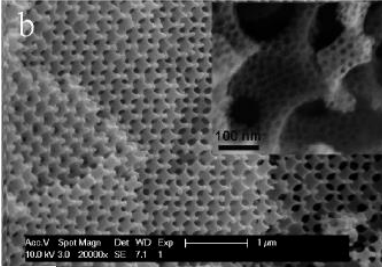
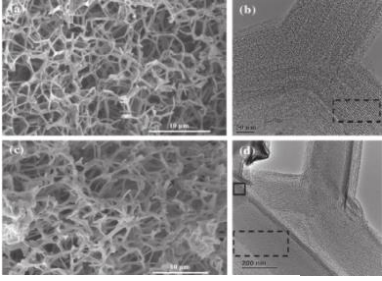
790 [97] Ng SWL, Yilmaz G, Ong WL, Ho GW. One-step activation towards spontaneous
791 etching of hollow and hierarchical porous carbon nanospheres for enhanced pollutant
792 adsorption and energy storage. *Appl Catal B Environ* 2018;220:533–41.
793 <https://doi.org/10.1016/J.APCATB.2017.08.069>.

794 [98] Zhang XQ, Cui YL, Zhong Y, Wang DH, Tang WJ, Wang XL, et al. Cobalt disulfide-
795 modified cellular hierarchical porous carbon derived from bovine bone for application
796 in high-performance lithium–sulfur batteries. *J Colloid Interface Sci* 2019;551:219–26.
797 <https://doi.org/10.1016/J.JCIS.2019.04.079>.

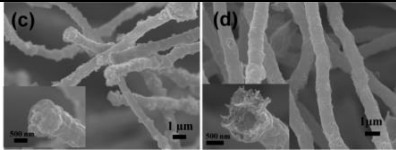
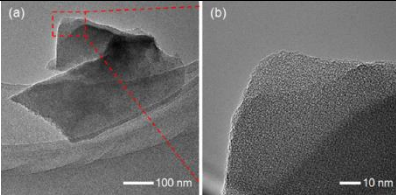
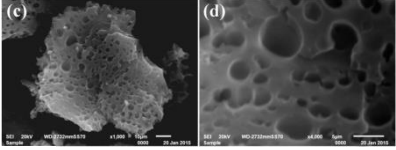
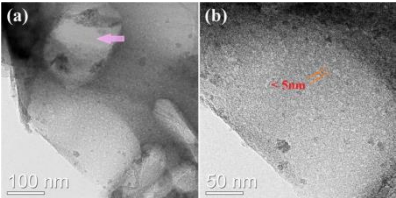
798 [99] Yun YS, Im C, Park HH, Hwang I, Tak Y, Jin H-J. Hierarchically porous carbon
799 nanofibers containing numerous heteroatoms for supercapacitors. *J Power Sources*
800 2013;234:285–91. <https://doi.org/10.1016/J.JPOWSOUR.2013.01.169>.
801

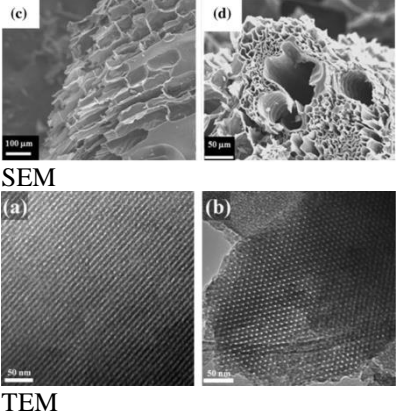
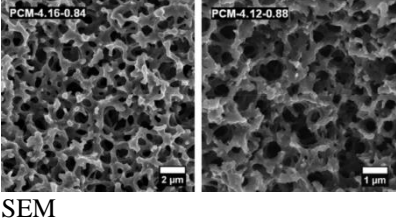
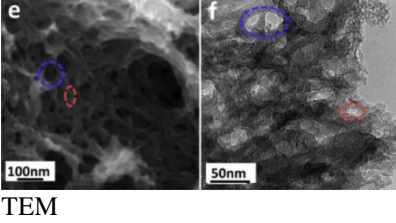
802 Table 1: Synthesis, properties and applications of HPCs.

Hierarchical porous carbon materials	Image (SEM, TEM)	Synthesis method	Properties	Application	Reference
Hierarchically macro-mesoporous monolithic carbon	 <p>SEM</p>	Dual-templating approach (nanocasting) with tri-block polymer F127 as the soft template, monolithic silica as hard template and resol as precursor	SSA=1036 m ² /g V (pore volume)=2.9 cm ³ g ⁻¹ Relatively disordered macro-mesopore size Macropore size about 2 μm Mesopore size about 7.08 nm	As super-capacitor materials	[34]
Hierarchically/bimodal macro-mesoporous carbon	 <p>SEM</p> <p>TEM</p>	Dual-templating approach with tri-block polymer F127 as the soft template, monodispersed silica colloidal crystal as the hard template and resols as precursor	SSA =760 m ² /g V (pore volume)=1.25 cm ³ g ⁻¹ Ordered macro-mesopore structure Macropore size about 230-430 nm Mesopore size about 11 nm Highly ordered face-centered cubic macrostructure Interconnected windows with a size of 30-65 nm		[36]
Hierarchically carbon spheres with hollow macroporous core and mesoporous shell	 <p>TEM</p> <p>SEM</p>	Dual-templating approach (aqueous route) with monodisperse silica spheres as hard template, F127 as soft template and resol as precursor	SSA =972 m ² g ⁻¹ V (pore volume)=1.27 cm ³ g ⁻¹ Macropore size about 250-300 nm Mesopore size 6–9 nm Thin shell thickness of 5 nm	As super-capacitors Highest capacitance (125 F g ⁻¹)	[35]

Dimensionally ordered macroporous carbon with mesoporous walls		Dual-templating approach with PS latex (macropore former and carbon source) and colloidal silica (mesopore former)	SSA = 1500 m ² g ⁻¹ V (pore volume) = 2.62 cm ³ g ⁻¹ A bimodal porous structure Mesopore size 5 nm Macropore size 190 nm	As electric double-layer capacitors [45] Showed highest capacitance of 120 F g ⁻¹	
SEM		Dual-templating approach one-pot method via in situ self-assembly of colloidal polymer (PMMA macropore former) and silica spheres (mesopore former) with sucrose as the carbon source	SSA = 818 m ² g ⁻¹ V (pore volume) = 1.29 cm ³ g ⁻¹ A bimodal porous structure Mesopore size 9 nm Macropore size 370 nm Small windows with a size of 120 nm	As a Catalyst Support [50] They show very good support of the Pt-Ru alloy catalyst in a direct methanol fuel cell.	
SEM	Hierarchically macro/mesoporous carbon monoliths		Nanocasting pathway by synthesizing parent SiO ₂ monolith (hydrothermal treatment, removal of P123 template and immerse into furfuryl alcohol solution) and carbon monoliths	SSA = 1354 m ² g ⁻¹ Hexagonal mesoporosity and three-dimensionally connected macroporosity Mesopore size 3.3-4 nm Macropore size 32.46 μm High macroporous cumulative volume is 48.6 cm ³ g ⁻¹ Regular cylindrical shape, strong hydrophobicity and low densities	As adsorbent [63] high adsorption capacity of 613 mg /g for bilirubin and oil with weight 23-48 times of their own in a few seconds.
SEM	TEM				

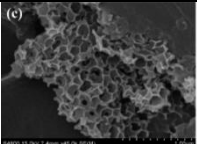
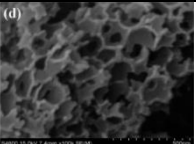
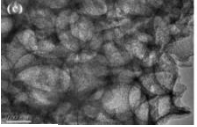
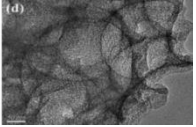
Hierarchically macro/mesoporous carbon		Dual-templating approach with SiO ₂ opal as a hard template, (F127 or P123) as a soft template, and phenolic resin as a precursor	SSA = 1667 m ² g ⁻¹ V (pore volume) = 4.80 cm ³ g ⁻¹ Highly periodic arrays of uniform and bimodal macropores with surrounding quasi-2D hexagonal mesoporous walls Mesopore size 18.1 nm Macropore size about 290 nm Interconnected windows with sizes of about 30 nm	[38]	
Hierarchically ordered macro-mesoporous carbon monoliths		dual-templating technique with poly (methyl methacrylate) (PMMA) colloidal crystals, F127 as soft templates and	SSA = 505 and 464 m ² g ⁻¹ V (pore volume) = 0.37 and 0.34 cm ³ g ⁻¹ Face-centered cubic and 2D-hexagonal mesoporous structure Mesopore size 2.7 nm and 3 nm Macropore size about 340 nm and 350 nm macropore window sizes of 150 nm and 130 nm	[51]	
The 1D hierarchical macro-mesoporous carbon nanofiber		Electrospinning pathway with polyacrylonitrile as carbon precursor and nano-CaCO ₃ as dual purpose template. Nano-CaCO ₃ template decomposed to released CO ₂ to develop mesopores, and CaO nanoparticles to develop	SSA = 123 m ² g ⁻¹ A total macropore volume of 18.7 cm ³ g ⁻¹ and a porosity degree of 50.4% Continuous and uniform nanofibers structure with winding mesopores The diameter of the nanofibers is 900 nm Pore size mainly distributed at	As catalyst support	[85]

	 <p>SEM</p>	macropores	4.2 nm	
Hierarchically disordered Micro-mesoporous carbon powder	 <p>TEM</p>	Carbonization and KOH activation by using corn cobs as the carbon resource with ultra-attenuation and purification by coupled ultrasonication-milling	$SSA = 2288 \text{ m}^2 \text{ g}^{-1}$ $V (\text{pore volume}) = 1.21 \text{ cm}^3 \text{ g}^{-1}$ With a high mesopore ratio of about 44.6% Average pore diameter 2.1 nm	As high-performance super-capacitor [86]
Hierarchical macroporous carbon foam with bicontinuous micro- mesoporous	 <p>SEM</p>  <p>TEM</p>	Carbonization and KOH activation by using glucose as the carbon resource	$SSA = 3106.7 \text{ m}^2 \text{ g}^{-1}$ $V (\text{pore volume}) = 1.82 \text{ cm}^3 \text{ g}^{-1}$ Typical amorphous structure and a block-like structure in micrometer scale The thickness of 5–10 nm Super-large macropores (0.5–5 μm) Bicontinuous large micropores (1.14 nm) Small mesopores (3.12 nm) With a high mesopore and micropore ratio of about 66.5% and 26.9%	Super-capacitor [87]

Hierarchically mesoporous monoliths	micro-carbon	 <p>SEM</p> <p>TEM</p>	Dual-templating approach with sugarcane bagasse as the scaffold, F127 as the soft template, and resol as carbon precursor	<p>SSA = 544 m² g⁻¹ V (pore volume) = 0.283 cm³ g⁻¹ 2-D hexagonal mesostructures and micrometer-sized lignocellulosic macroporous texture Enhanced degree of graphitization Mesopore size about 3 nm Micropore size about 0.5 nm Micropore percentages of 66–67%.</p>	As capacitances [53] Show good electrochemical property and the specific capacitances are in the range 190–234 F g ⁻¹
Hierarchically macroporous and mesoporous monoliths	micro-carbon	 <p>SEM</p>	Phase separation induced by polymerization of resorcinol and formaldehyde to produce macropores or mesopores, and CO ₂ activation to produce micropores	<p>SSA = 1000-2400 m² g⁻¹ V (pore volume) = 0.4-0.92 cm³/g No regularly arranged structures in the mesopore size range. Macro- and mesopores size were tailored from approximately 10 μm to 2 mm With a low degree of graphitization</p>	As CO ₂ adsorption capacity [88]
Hierarchical mesoporous monolith	macro-carbon	 <p>TEM</p>	Dual-templating approach with P123 as soft template, mesoporous silica (KIT-6) as hard template and lignin as carbon precursor	<p>SSA = 803 m² g⁻¹ V (pore volume) = 0.86 cm³ g⁻¹ A well-interconnected 3D porous network Mesopore size about 3.4, 6.4 and about 50 nm Macropore size about 100 nm The thick of carbon monolith is 310 μm</p>	As the high-performance electrode for electric double layer supercapacitor. [49]

Hierarchically micro/mesoporous carbons		<p>“Nanopore lithography” strategy by graphene oxide (GO) nanosheets enclosing ZIF-8 particles as templates to produce mesoporous structure</p>	<p>SSA = 1300 -1350 m² g⁻¹ V (pore volume) = 1.1-1.2 cm³ g⁻¹ Mesopore size about 3-4 nm</p>	<p>As electrochemical energy storage [59]</p>
Hierarchical macro-meso-microporous carbon monolith		<p>Template-free approach by ultrasonic irradiation to produce macropores, Ca(NO₃)₂ impregnation followed by CO₂ activation to produce mesopores and resorcinol-formaldehyde as carbon precursor</p>	<p>SSA = 624 m² g⁻¹ Slit-pore shape of mesopore and not well-defined mesopore size distribution Mean pore size diameter of 1.2 μm Mesopore volume of 0.38 cm³ g⁻¹ Micropore volume of 0.22 cm³ g⁻¹</p>	<p>[60]</p>
Three-dimensionally disordered interconnected micro-, meso- and macropores carbon		<p>Template-free approach by constructing carbonyl crosslinking bridges between polystyrene chains</p>	<p>SSA = 679 m² g⁻¹ S (micropore surface area) = 390 m² g⁻¹ V (pore volume) = 0.66 cm³ g⁻¹ Micro-, meso-, macropore volumes account for 32%, 56% and 12% Mesopore size < 2 nm Mesopore size about 2-50 nm Macropore size about 50-400 nm</p>	<p>[61]</p>

<p>Ordered, uniform, macroporous carbons with mesoporous walls</p>		<p>Dual-templating approach by mixing monodisperse polystyrene spheres and silica particles with divinylbenzene as carbon precursor</p>	<p>SSA = 465 m² g⁻¹ V (pore volume) = 1.32 cm³ g⁻¹ Periodically ordered, bimodal porous carbon Mesopore size about 10 nm Macropore size about 317 nm Interconnected windows with a size of 110 nm</p>	<p>As Catalyst Supports in Direct Methanol Fuel Cells [44]</p>
<p>Hierarchical micro-mesoporous carbons</p>		<p>Template carbonization and CO₂ activation by using CMK-3 and CMK-1 as mesoporous template</p>	<p>SSA = 2749 and 2696 m² g⁻¹ V (pore volume) = 2.09 and 1.87 cm³ g⁻¹ V (micropore volume) = 0.96 and 0.94 cm³ g⁻¹ V (mesopore volume) = 1.13 and 0.93 cm³ g⁻¹ Mesopore size about 3-4 nm</p>	<p>As super-capacitor electrode materials [57]</p>
<p>Hierarchical /meso-macroporous carbon aerogel monoliths</p>		<p>Sol-gel polymerization to produce macroporous carbon aerogel and CO₂ activation to produce mesopores or micropores</p>	<p>SSA = 1500-3000 m² g⁻¹ V (pore volume) = 0.78-1.88 cm³ g⁻¹ V (micropore volume) = 0.583 cm³ g⁻¹ Carbon aerogel monoliths with densities about 0.55 g cm⁻³</p>	<p>[89]</p>

Hierarchical interconnected meso-macroporous carbon	 SEM	   TEM	<p>Template carbonization by using silica nanospheres as macroporous template and KOH activation to produce mesopores and micropores</p>	<p>SSA = 2784 m² g⁻¹ V (pore volume) = 1.382 cm³ g⁻¹ A three-dimensional continuous cellular-like structure V (micropore volume) = 0.678 cm³ g⁻¹ D (average size) = 2.155 nm Mesopore size about 3-4 nm Macroporous diameter of about 200 nm The presence of a few graphite structure in the carbon framework</p>	As adsorbent for [79] sulfamethazine
---	--	--	--	--	--------------------------------------

803

804

805 Table 2: Use of HPCs and modified HPCs in organic contaminant removal from water and wastewater.

Hierarchical porous carbon material	Carbon precursor	Modification	Organic contaminant	Contaminant concentration	Background solution		Adsorption capacity	Adsorption mechanism	Reference
					Ionic strength	pH			
Hierarchically macro/mesoporous carbon monoliths	Tetraethoxysilane	-	Bilirubin	200 mg L ⁻¹	0.2 M NaOH solution	7.4	613 mg g ⁻¹	Hierarchically porous structure	[63]
Hierarchical 3D interconnected micro-meso-macroporous carbon	sodium lignin sulfonate	KOH activation	Sulfamethazine	Initial concentrations of 50, 80, 120, 160, 200, 250, and 300 mg L ⁻¹	2.0 mg of 3DLHPC was mixed with 10 mL of SMZ solution (C ₀ = 160 mg L ⁻¹) with the humic acid concentration of 10, 25, 50, and 100 mg L ⁻¹ , respectively.	3.0–9.0	869.6 mg g ⁻¹	Mainly due to the higher specific surface area and pore volume, Partly van der Waals force, π - π EDA interaction, electronic interaction, hydrophobic interaction, and hydrogen bonding interaction	[79]
Hierarchical porous carbons well-defined hollow tubular structures in nano-size with micro-mesoporous	sodium lignin sulfonate	KOH activation	Tetracycline	Initial concentrations in a range of 50–400 mg L ⁻¹	Na ⁺ , K ⁺ , Ca ²⁺ , Fe ³⁺ , Co ²⁺ (0.01 M), and humic acid (5–50 mg L ⁻¹)	3–8 for TC (250 mg L ⁻¹)	1297.0 mg g ⁻¹	oxygen containing functional groups	[80]

Hierarchical porous carbons well-defined hollow tubular structures in nano-size with micro-mesoporous	sodium lignin sulfonate	KOH activation	Chloramphenicol	Initial concentrations in a range of 20–200 mg L ⁻¹	Na ⁺ ,K ⁺ ,Ca ²⁺ ,Fe ³⁺ ,Co ²⁺ (0.01 M), and humic acid (5–50 mg L ⁻¹)	3–11 for CAP (200 mg L ⁻¹)	1067.2 mg g ⁻¹	oxygen containing functional groups	[80]
Ferromagnetic hierarchical porous carbon	phenolic resin	-	Methylene orange	1.5 x 10 ⁴ M	water		0.16 mg m ⁻²	the strong pore surface-molecule electrostatic force and volume filling effect	[90]
Macro-meso-micro hierarchical porous carbon	bovine bone	KOH activation	Sulfamethazine	200 mg L ⁻¹	water	-	1194 mg g ⁻¹		[78]
Macro-meso-micro hierarchical porous carbon	bovine bone	KOH activation	Chloramphenicol	200 mg L ⁻¹	water	-	1240 mg g ⁻¹		[78]
Hierarchical macroporous carbon with the mesopores and size-uniform wormhole-like micropores	Furfuryl alcohol	-	Methylene blue	500 mg L ⁻¹	water	-	250 mg g ⁻¹	hierarchically porous structure	[77]
Microporous or micro-mesoporous or micro-meso-macroporous carbon	prepared by sol-gel process from Resorcin	-	Phenol	1mM		-		hierarchically porous structure	[83]

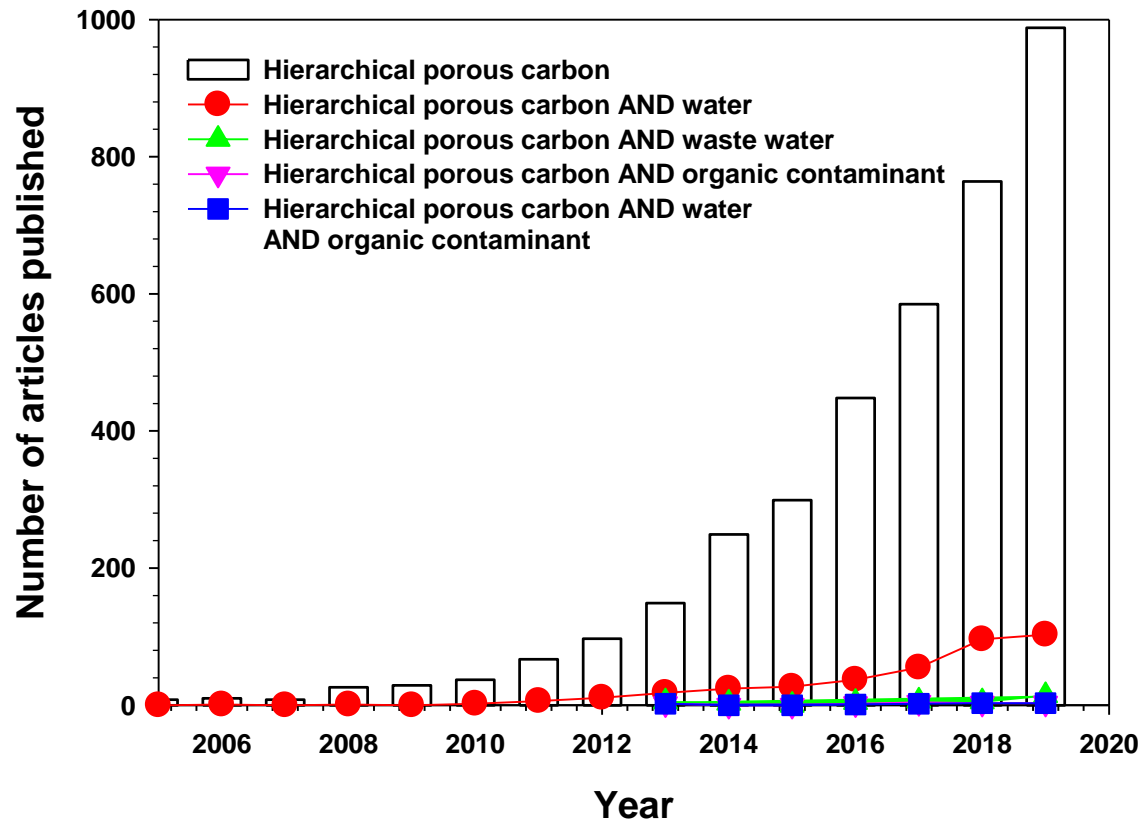
materials	ol and formaldehyde								
Hierarchically ordered mesoporous carbon	Tetraethyl orthosilicate	-	Bisphenol A	345 mg L ⁻¹	ethanol	-	1106 mg g ⁻¹	hierarchically porous structure	[81]
Hierarchical porous N-doped carbon microspheres	pomelo peel	-	Rhodamine B	20 mg L ⁻¹	Water	-	249.8 mg g ⁻¹	superhydrophilic surfaces	[91]
Hierarchical porous N-doped carbon microspheres	pomelo peel	-	Methyl orange	20 mg L ⁻¹	Water	-	416.3 mg g ⁻¹	superhydrophilic surfaces	[91]
Hierarchical porous N-doped carbon microspheres	pomelo peel	-	Rhodamine 6G	20 mg L ⁻¹	Water	-	120 mg g ⁻¹	superhydrophilic surfaces	[91]
Heteroatom (nitrogen and sulfur)-codoped porous carbons (N-SPCs) N-S-PC-2 (15% thiourea)	Glucose	-	Sulfachloropyridazine	20 mg L ⁻¹		7	220 mg g ⁻¹	well-defined pore structure Synergetic effect of N and S	[25]
Heteroatom (nitrogen and sulfur)-codoped porous carbons (N-SPCs) N-S-PC-1 (5% thiourea)	Glucose	-	Sulfachloropyridazine	20 mg L ⁻¹		7	190 mg g ⁻¹	well-defined pore structure	[25]

Heteroatom (nitrogen and sulfur)-codoped porous carbons (N-SPCs) N-S-PC-3 (25% thiourea)	Glucose	-	Sulfachloropyridazine	20 mg L ⁻¹	7	126 mg g ⁻¹			well-defined pore structure	[25]
Nitrogen doped activated porous carbon fibers (FeCo ₂ @APC Fs)	polyacrylonitrile/polybenzoxazine	KOH activation	Methylene blue	20 mg L ⁻¹	-	99.08% efficiency	removal within 25 min		High surface area, Activation of peroxymonosulfate with reactive oxygen radicals (SO ₄ ^{•-} , [•] OH, and ¹ O ₂)	[92]
Nitrogen doped activated porous carbon fibers (FeCo ₂ @APC Fs)	polyacrylonitrile/polybenzoxazine	KOH activation	Sulfamethoxazole	20 mg L ⁻¹		68.8% efficiency	removal within 25 min		High surface area, Activation of peroxymonosulfate with reactive oxygen radicals (SO ₄ ^{•-} , [•] OH, and ¹ O ₂)	[92]
Nitrogen doped activated porous carbon fibers (FeCo ₂ @APC Fs)	polyacrylonitrile/polybenzoxazine	KOH activation	Phenol	20 mg L ⁻¹		62.28% efficiency	removal within 25 min		High surface area, Activation of peroxymonosulfate with reactive oxygen radicals (SO ₄ ^{•-} , [•] OH, and ¹ O ₂)	[92]
Nitrogen doped activated porous carbon fibers (FeCo ₂ @APC Fs)	polyacrylonitrile/polybenzoxazine	KOH activation	Bisphenol-A	20 mg L ⁻¹		53.76% efficiency	removal within 25 min		High surface area, Activation of peroxymonosulfate with reactive oxygen radicals (SO ₄ ^{•-} , [•] OH, and ¹ O ₂)	[92]

Fs)								¹ O ₂)	
Nitrogen doped activated porous carbon fibers (FeCo ₂ @APC Fs)	polyacrylonitrile/polybenzoxazine	KOH activation	Chlorophenol	20 mg L ⁻¹		63.96% efficiency	removal within 25 min	High surface area, Activation of peroxymonosulfate with reactive oxygen radicals (SO ₄ ^{•-} , [•] OH, and ¹ O ₂)	[92]

806

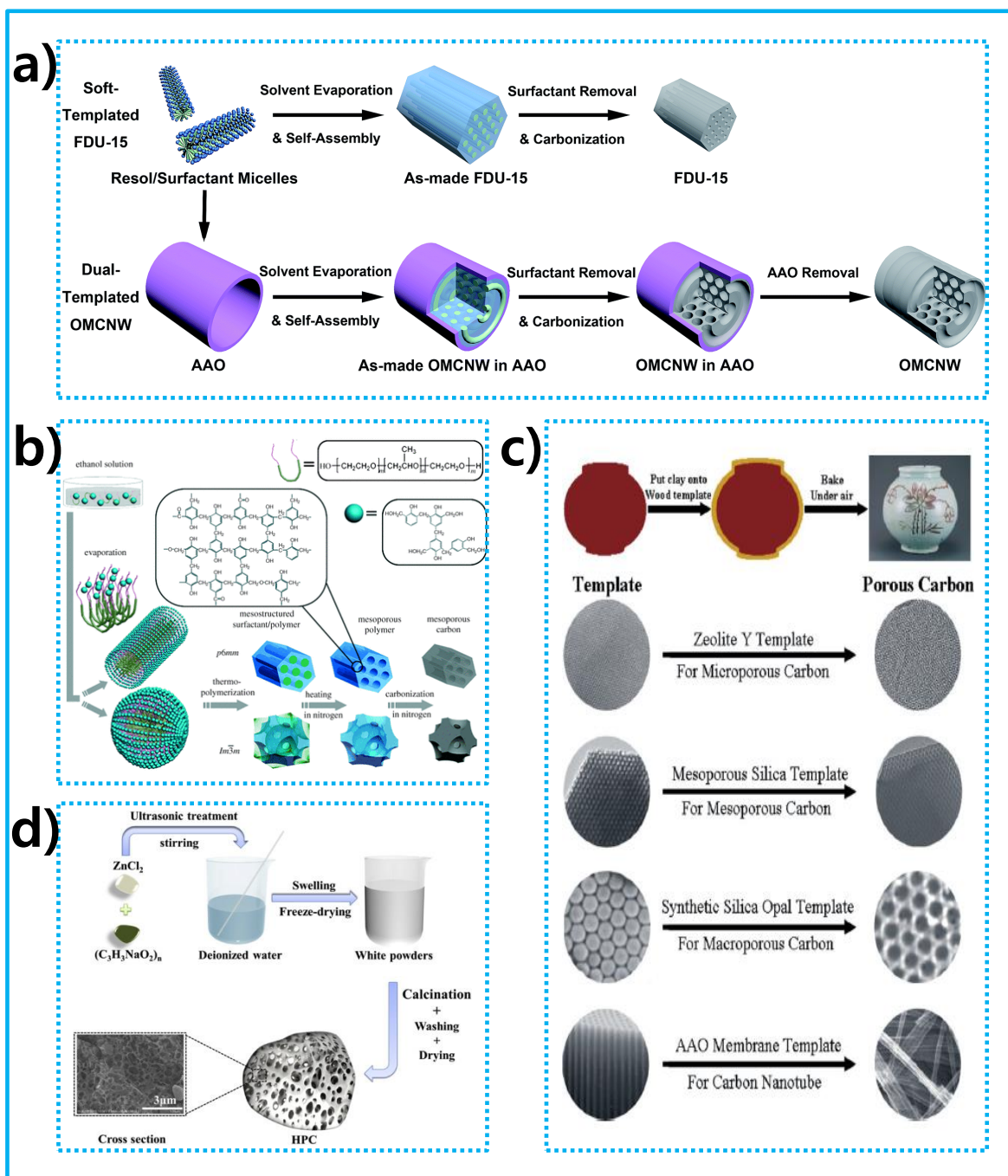
807



808

809 Fig. 1: Bibliometric analysis of SCOPUS database publications on hierarchical porous carbons, organic contaminant, wastewater and water

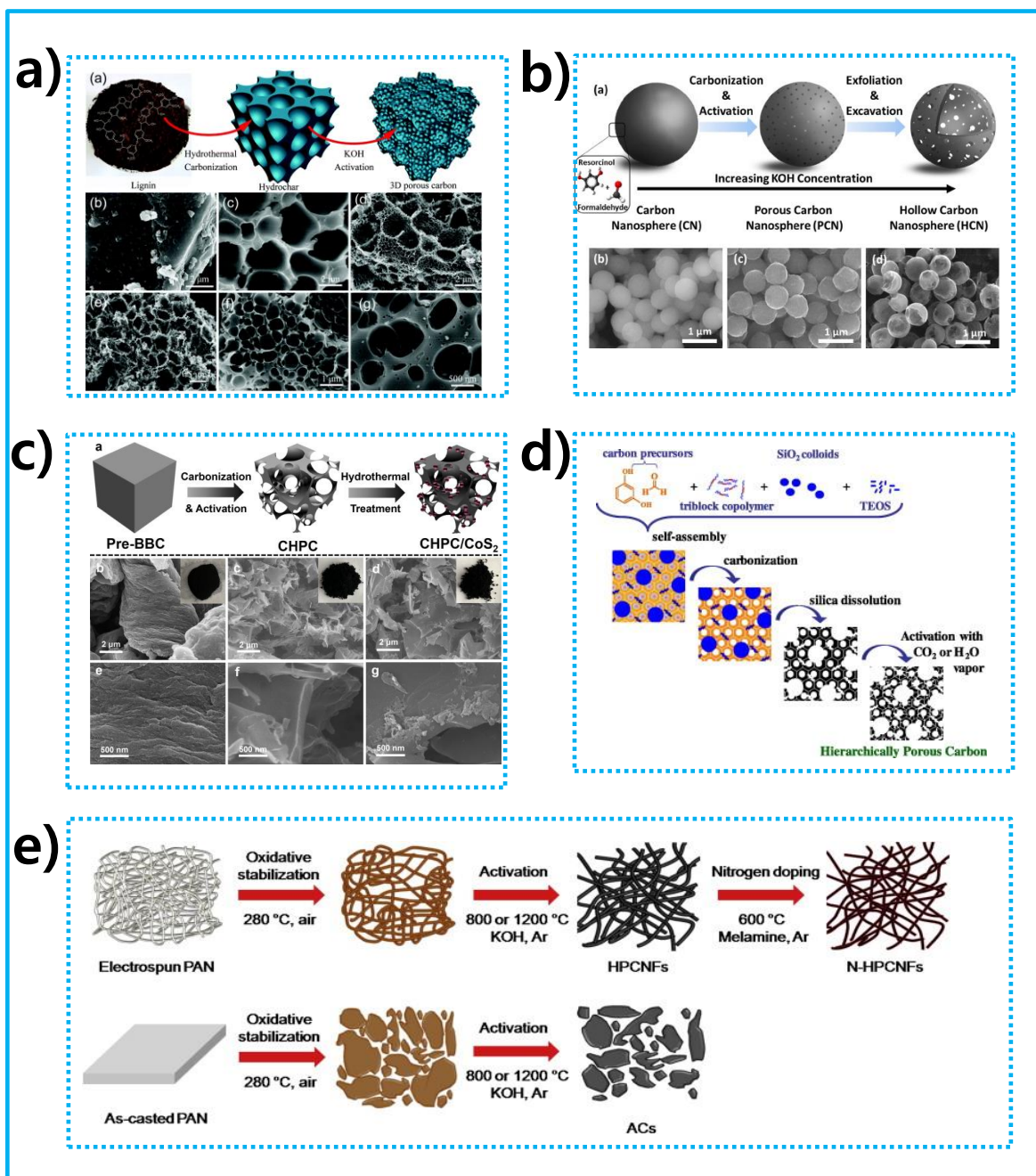
810 (quoted on 15 January 2020)



811

812 Fig. 2: Synthesis routes for HPCs using a) soft template and dual template [93], b) soft
 813 template [47], c) hard template [94], and d) multiple templates fabrication [95].

814



815

816 Fig. 3: Schematic illustration of a) KOH activation [96], b) KOH activation with increasing
 817 concentrations [97], c) KOH and hydrothermal activations and corresponding SEM images
 818 [98], d) CO₂ and H₂O activations [74], and e) KOH activation, temperature treatments and
 819 nitrogen doping [99].